Updated 09/04/2020

Supporting Information For

Trends in Trigonal Prismatic Ln-[1]ferrocenophane Complexes Complexes and Discovery of a Ho^{3+} Single-Molecule Magnet

Trevor P. Latendresse, Veacheslav Vieru, Apoorva Upadhyay, Nattamai S. Bhuvanesh, Liviu F. Chibotaru, and Michael Nippe

Table of Contents

Crystallography

Data Collection …… **S4**
Data Reduction, Structure Solution, and Refinement …… **S4**

Table S1. Crystallographic data for **1** …… **S5**
Fig. S1. Molecular structure of **1** …… **S5**
Table S2. Crystallographic data for **2** …… **S6**
Fig. S2. Molecular structure of **2** …… **S6**
Table S3. Crystallographic data for **2-py** …… **S7**
Fig. S3. Molecular structure of **2-py** …… **S7**
Table S4. Crystallographic data for **2-THF*** …… **S8**
Fig. S4. Molecular structure of **2-THF*** …… **S8**
Table S5. Crystallographic data for **3** …… **S9**
Fig. S5. Molecular structure of **3** …… **S9**
Table S6. Crystallographic data for **4** …… **S10**
Fig. S6. Molecular structure of **4** …… **S10**
Table S7. Crystallographic data for **5** …… **S11**
Fig. S7. Molecular structure of **5** …… **S11**
Table S8. Crystallographic data for $\mathbf{5^{Iso}}$ …… **S12**
Fig. S8. Molecular structure of $\mathbf{5^{Iso}}$ …… **S12**
Table S9. Crystallographic data for **6** …… **S13**
Fig. S9. Molecular structure of **6** …… **S13**
Table S10. Crystallographic data for $\mathbf{6^{Iso}}$ …… **S14**
Fig. S10. Molecular structure of $\mathbf{6^{Iso}}$ …… **S14**
Table S11. Selected Interatomic distances and angles for **1-6** …… **S15**
Table S12. Selected Interatomic distances and angles for $\mathbf{5^{Iso}}$ and $\mathbf{6^{Iso}}$ …… **S16**
Table S13. Selected Interatomic distance and angles for **2-py** and **2-THF*** …… **S17**
Table S14. Closest intermolecular distances for **2**, **2-py**, **2-THF*** …… **S18**

Magnetism

Static Magnetic Properties

Fig. S11. $\chi_M T$ vs. T plot for **2-py**…… **S19**
Fig. S12. M vs. H plots of **1-5/5^{Iso}**…… **S19**
Fig. S13. M vs. H/T plots of **1-5/5^{Iso}**…… **S20**
Fig. S14. M vs. H plots of **2-py**…… **S20**
Fig. S15. M vs. H/T plots of **2-py**…… **S21**
Fig. S16. Hysteresis plots of **2**…… **S21**

Dynamic Magnetic Properties

Fig. S17. χ_M' vs. Frequency plot of **2** (H = 0 T)…… **S22**
Fig. S18. χ_M'' vs. Frequency plots of resolved **2** (T = 2K - 7K, H = 0T)…… **S23**
Fig. S19. χ_M'' vs. Frequency plots of resolved **2** (T = 8K - 11K, H = 0T)…… **S24**
Fig. S20. χ_M' vs. Frequency plots of resolved **2** (T = 2K - 7K, H = 0T)…… **S25**
Fig. S21. χ_M' vs. Frequency plots of resolved **2** (T = 8K - 11K, H = 0T)…… **S26**
Fig. S22. χ_M' vs. Frequency plot of resolved SR of **2** (H = 0T)…… **S27**
Fig. S23. χ_M' vs. Frequency plot of resolved FR of **2** (H = 0T)…… **S27**
Fig. S24. Cole-Cole plot of **2** (H = 0T)…… **S28**
Table S15. Cole-Cole fitting parameters for **2** (H = 0T)…… **S28**
Fig. S25. χ_M'' vs. Frequency plot of **2** (H = 0.02T – 0.35T, T = 8K)…… **S29**
Fig. S26. χ_M' vs. Frequency plot of **2** (H = 0.02T – 0.35T, T = 8K)…… **S29**
Fig. S27. χ_M'' vs. Frequency plot of **2** (H = 0.4T – 2T, T = 8K)…… **S30**
Fig. S28. χ_M' vs. Frequency plot of **2** (H = 0.4T – 2T, T = 8K)…… **S30**
Fig. S29. Cole-Cole plot of **2** (H = 0.02T – 0.35T, T = 8K)…… **S31**
Fig. S30. Cole-Cole plot of **2** (H = 0.4T – 2T, T = 8K)…… **S31**
Fig. S31. τ vs. H plot of **2** (H = 0T – 2T, T = 8K)…… **S32**
Fig. S32. χ_M' vs. Frequency plot of **2** (H = 0.35 T)…… **S32**
Fig. S33. Cole-Cole plot of **2** (H = 0.35 T)…… **S33**
Table S16. Cole-Cole fitting parameters for **2** (H = 0.35 T)…… **S33**
Fig. S34. χ_M' vs. Frequency plot of **2-dilute** (H = 0T) …… **S34**
Fig. S35. χ_M'' vs. Frequency plots of resolved **2-dilute** (T = 2K - 7K, H = 0T)…… **S35**
Fig. S36. χ_M'' vs. Frequency plots of resolved **2-dilute** (T = 8K - 11K, H = 0T)…… **S36**
Fig. S37. χ_M' vs. Frequency plots of resolved **2-dilute** (T = 2K - 7K, H = 0T)…… **S37**
Fig. S38. χ_M' vs. Frequency plots of resolved **2-dilute** (T = 8K - 11K, H = 0T)…… **S38**
Fig. S39. χ_M' vs. Frequency plot of resolved SR of **2-dilute** (H = 0T)…… **S39**
Fig. S40. χ_M' vs. Frequency plot of resolved FR of **2-dilute** (H = 0T)…… **S39**
Fig. S41. Cole-Cole plot of **2-dilute** (H = 0T)…… **S40**

Table S17. Cole-Cole fitting parameters for **2-dilute** (H = 0T)……..…… **S40**
Fig. S42. χ_M' vs. Frequency plot of **2-py** (H = 0T) …… **S41**
Fig. S43. χ_M'' vs. Frequency plot of **5** (H = 0.02T – 0.08T, T = 2K)……. **S42**
Fig. S44. χ_M'' vs. Frequency plot of **5** (H = 0.1T – 0.35T, T = 2K)……... **S42**
Fig. S45. χ_M' vs. Frequency plot of **5** (H = 0.02T – 0.08T, T = 2K)…….. **S43**
Fig. S46. χ_M' vs. Frequency plot of **5** (H = 0.1T – 0.35T, T = 2K)…… **S43**
Fig. S47. Cole-Cole plot of **5** (H = 0.02T – 0.08T, T = 2K)…….……..… **S44**
Fig. S48. Cole-Cole plot of **5** (H = 0.1T – 0.35T, T = 2K)…….…… **S44**
Fig. S49. τ vs. H plot of **5** (H = 0T – 0.35T, T = 2K)……...…….. **S45**
Fig. S50. χ_M' vs. Frequency plot of **5** (H = 0.2T)…….…….. **S45**
Fig. S51. Cole-Cole plot of **5** (H = 0.2 T)……..……. **S46**
Table S18. Cole-Cole fitting parameters for **5/5^{Iso}** (H = 0.2T)……... **S46**
Table S19. Arrhenius fitting parameters for **5/5^{Iso}** where H = 0.2 T…….…. **S46**

<u>Ab Initio Calculations</u>

Computational Details

Table S20. Employed Basis Sets For **2-5**……..……..…… **S47**
Table S21. Energy of low-lying Ising doublets of **2**.……..… **S48**
Table S22. The **g**-tensor of the lowest four doublets of **2**.……..… **S48**
Table S23. Energy of low-lying Kramers doublets of **3**.……..…….. **S49**
Table S24. The **g**-tensor of the lowest four doublets of **3**.……..… **S49**
Table S25. Energy of low-lying Ising doublets of **4**.……..…… **S50**
Table S26. Energy of low-lying Kramers doublets of **5**. …….….…… **S50**
Table S27. The **g**-tensor of the lowest four doublets of **5**. ……...… **S51**
Fig. S52. Experimental vs. calculated χ_MT vs. T plot of **2**. ……...…… **S52**
Fig. S53. Experimental vs. calculated χ_MT vs. T plot of **3**. ……...……..…..… **S52**
Fig. S54. Experimental vs. calculated χ_MT vs. T plot of **4**. ……...…… **S53**
Fig. S55. Experimental vs. calculated χ_MT vs. T plot of **5**. ……...……..…..… **S53**
Fig. S56. Experimental vs. calculated M vs. H curves of **2-5**. ……..…… **S54**
Fig. S57. Experimental vs. calculated M vs. H/T curves of **2-5**. …….….. **S54**

References…….…. **S55**

Crystallography:

Data Collection

A Leica MZ 75 microscope was used to identify a crystal suitable for X-ray analysis. The crystal mounted on a nylon loop which was then placed in a cold nitrogen stream (Oxford) maintained between 100 - 120 K.

A BRUKER Quest X-ray (fixed-Chi geometry) diffractometer was employed for crystal screening, unit cell determination, and data collection. The goniometer was controlled using the APEX3 software suite.[1] The sample was optically centered with the aid of a video camera such that no translations were observed as the crystal was rotated through all positions. The X-ray radiation employed was generated from a Mo-Iμs X-ray tube (K_α = 0.71073Å).

45 data frames were taken at widths of 1°. These reflections were used to determine the unit cell. The unit cell was verified by examination of the *h k l* overlays on several frames of data. No super-cell or erroneous reflections were observed. For compounds **1-6** the unit cell showed two short and one extremely long (> 60 Å) axes, causing significant overlap. The data was, hence, collected at a crystal to detector length between 200-220 mm, to better resolve the peaks. After careful examination of the unit cell, an extended data collection procedure was initiated using omega scans.

Data Reduction, Structure Solution, and Refinement

Integrated intensity information for each reflection was obtained by reduction of the data frames with the program APEX3.[1] The integration method employed a three dimensional profiling algorithm and all data were corrected for Lorentz and polarization factors, as well as for crystal decay effects. Finally, the data was merged and scaled to produce a suitable data set. The absorption correction program SADABS[2] was employed to correct the data for absorption effects. For compounds **1-3** and **6** not many reflections were observed above 40 degrees two-theta; final least squares refinement was restricted to that angle.

A solution was obtained readily using XT/XS in APEX3.[1,3] Hydrogen atoms were placed in idealized positions and were set riding on the respective parent atoms. All non-hydrogen atoms were refined with anisotropic thermal parameters. For compounds **1-6**, thermal ellipsoids on two of the THFs indicated strong possibility of disorder which were modeled between two positions each with occupancy ratio of 0.62:0.38 and 0.71:0.29 (for **1**), 0.77:0.23 and 0.66:0.34 (for **2**), 0.72:0.28 and 0.53:0.47 (for **3**), 0.63:0.37 and 0.51:0.49 (for **4**) and 50:50 and 60:40 (for **6**). Appropriate restraints and / or constraints were added to keep the bond distances, angles, and thermal ellipsoids meaningful. Several atoms showed unusual thermal ellipsoids (flattened, or non-positive definites); restraints or constraints were added to make them meaningful. Absence of additional symmetry and voids were confirmed using PLATON (ADDSYM).[4] The structure was refined (weighted least squares refinement on F^2) to convergence.[3,5] Olex2 was employed for the final data presentation and structure plots.[5]

Table S1. Crystallographic Data for $[Li(THF)_4][GdFc_3(THF)_2Li_2]$ **(1)**.

Compound	**$\{Gd[(C_5H_4)_2Fe]_3[Li(THF)]_2\}\cdot Li(THF)_4$**
Formula	$C_{54}H_{72}GdFe_3Li_3O_6$
Crystal system	monoclinic
Space group	$P2_1/c$
a, Å	11.3774(12)
b, Å	63.872(7)
c, Å	13.7293(15)
α,°	90
β,°	92.491(4)
γ, °	90
Volume, $Å^3$	9967.6(18)
Z	8
T, K	110.0
ρ_{calcd} (mg/m^3)	1.550
F(000)	4760
θ_{min}, θ_{max}, °	2.179, 24.999
R_1^a, wR_2^b ($I > 2\sigma(I)$)	0.0685, 0.1267
R_1^a, wR_2^b (all data)	0.0802, 0.1323

$^aR_1 = 3||F_o|-|F_c||/3|F_o|$. $^bwR_2 = [3[w(F_o^2 - F_c^2)^2]/3[w(F_o^2)^2]]^{½}$, $w = 1/\sigma^2(F_o^2) + (aP)^2 + bP$, where $P = [\max(0 \text{ or } F_o^2) + 2(F_c^2)]/3$.

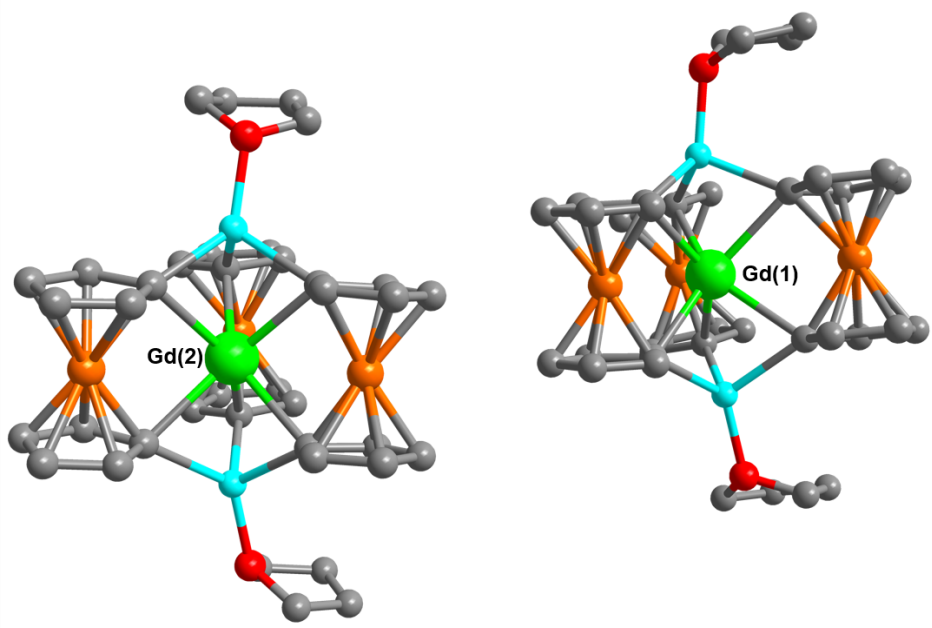

Fig. S1. Molecular structure of two independent molecules of monoanionic **1**. Atom labels are green = Gd, orange = Fe, light blue = Li, red = O, and grey = C. Hydrogen atoms and counter cations removed for clarity.

Table S2. Crystallographic Data for $[Li(THF)_4][HoFc_3(THF)_2Li_2]$ **(2)**.

Compound	**$\{Ho[(C_5H_4)_2Fe]_3[Li(THF)]_2\}\cdot Li(THF)_4$**
Formula	$C_{54}H_{72}HoFe_3Li_3O_6$
Crystal system	monoclinic
Space group	$P2_1/c$
a, Å	11.3991(7)
b, Å	63.596(3)
c, Å	13.7285(8)
α,°	90
β,°	92.383(2)
γ, °	90
Volume, $Å^3$	9943.8(10)
Z	8
T, K	100
ρ_{calcd} (mg/m^3)	1.564
F(000)	4784
θ_{min}, θ_{max}, °	2.184, 22.500
$R_1{}^a$, $wR_2{}^b$ ($I > 2\sigma(I)$)	0.0848, 0.1426
$R_1{}^a$, $wR_2{}^b$ (all data)	0.1061, 0.1511

$^aR_1 = 3||F_o|-|F_c||/3|F_o|$. $^bwR_2 = [3[w(F_o^2 - F_c^2)^2]/3[w(F_o^2)^2]]^{½}$, $w = 1/\sigma^2(F_o^2) + (aP)^2 + bP$, where $P = [\max(0 \text{ or } F_o^2) + 2(F_c^2)]/3$.

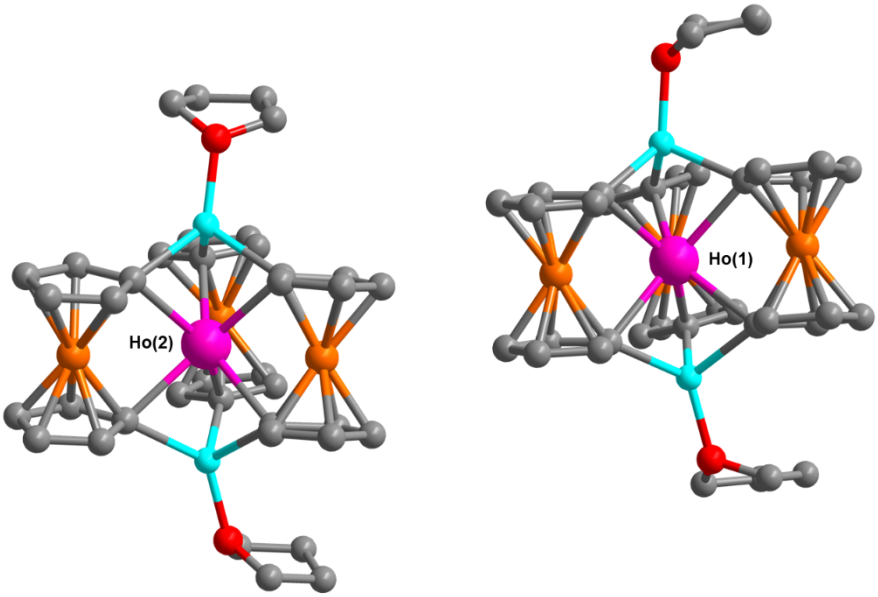

Fig. S2. Molecular structure of two independent molecules of monoanionic **2**. Atom labels are pink = Ho, orange = Fe, light blue = Li, red = O, and grey = C. Hydrogen atoms and counter cations removed for clarity.

Table S3. Crystallographic Data for $[Li(py)_4][HoFc_3(py)_2Li_2]$ **(2-py)**.

Compound	**$\{Ho[(C_5H_4)_2Fe]_3[Li(py)]_2\}\cdot Li(THF)_4$**
Formula	$C_{64.38}H_{58.38}HoFe_3Li_3N_{6.88}$
Crystal system	Orthorhombic
Space group	$P2_12_12_1$
a, Å	21.2060(9)
b, Å	22.6446(10)
c, Å	23.1321(11)
α,°	90
β,°	90
γ, °	90
Volume, $Å^3$	11108.1(9)
Z	8
T, K	110
ρ_{calcd} (mg/m^3)	1.533
F(000)	5174
θ_{min}, θ_{max}, °	1.303, 24.999
R_1^a, wR_2^b ($I > 2\sigma(I)$)	0.0494, 0.0932
R_1^a, wR_2^b (all data)	0.0920, 0.1135

$^aR_1 = 3||F_o|-|F_c||/3|F_o|$. $^bwR_2 = [3[w(F_o^2 - F_c^2)^2]/3[w(F_o^2)^2]]^{½}$, $w = 1/\sigma^2(F_o^2) + (aP)^2 + bP$, where $P = [\max(0 \text{ or } F_o^2) + 2(F_c^2)]/3$.

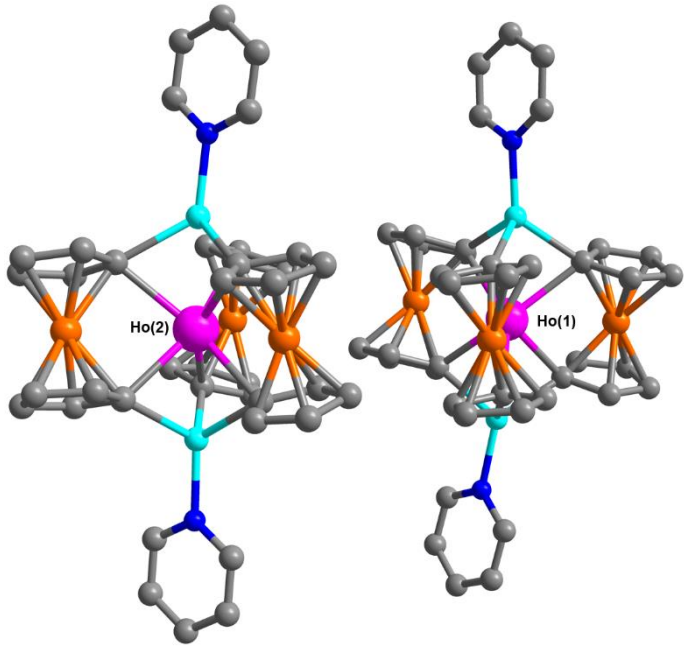

Fig. S3. Molecular structure of two independent molecules of monoanionic **2-py**. Atom labels are pink = Ho, orange = Fe, light blue = Li, dark blue = N, and grey = C. Hydrogen atoms, counter cations, and pyridine solvate molecules removed for clarity.

Table S4. Crystallographic Data for $[Li(THF^*)_4][HoFc_3(THF^*)_2Li_2]$ **(2-THF*)**.

Compound	**$\{Ho[(C_5H_4)_2Fe]_3[Li(THF^*)]_2\}\cdot Li(THF)_4$**
Formula	$C_{60}H_{84}Fe_3HoLi_3O_6$
Crystal system	Monoclinic
Space group	$P2_1/n$
a, Å	11.3389(4)
b, Å	13.7172(5)
c, Å	36.2329(12)
α,°	90
β,°	95.3440(10)
γ, °	90
Volume, $Å^3$	5611.1(3)
Z	4
T, K	110
ρ_{calcd} (mg/m^3)	1.485
F(000)	2584
θ_{min}, θ_{max}, °	2.336, 24.999
R_1^a, wR_2^b ($I > 2\sigma(I)$)	0.0931, 0.1648
R_1^a, wR_2^b (all data)	0.0998, 0.1666

$^aR_1 = 3||F_o|-|F_c||/3|F_o|$. $^bwR_2 = [3[w(F_o^2 - F_c^2)^2]/3[w(F_o^2)^2]]^{½}$, $w = 1/\sigma^2(F_o^2) + (aP)^2 + bP$, where $P = [\max(0 \text{ or } F_o^2) + 2(F_c^2)]/3$.

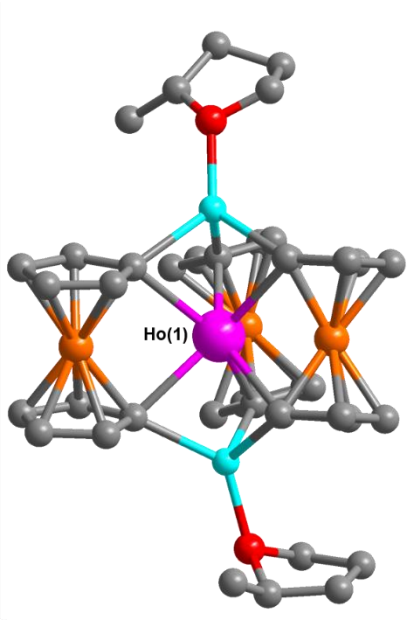

Fig. S4. Molecular structure of two independent molecules of monoanionic **2-THF***. Atom labels are pink = Ho, orange = Fe, light blue = Li, red = O, and grey = C. Hydrogen atoms and counter cations removed for clarity.

Table S5. Crystallographic Data for $[Li(THF)_4][ErFc_3(THF)_2Li_2]$ **(3)**.

Compound	**$\{Er[(C_5H_4)_2Fe]_3[Li(THF)]_2\}\cdot Li(THF)_4$**
Formula	$C_{54}H_{72}ErFe_3Li_3O_6$
Crystal system	monoclinic
Space group	$P2_1/c$
a, Å	11.4007(11)
b, Å	63.598(6)
c, Å	13.7293(14)
α,°	90
β,°	92.262(4)
γ, °	90
Volume, $Å^3$	9946.9(17)
Z	8
T, K	110.0
ρ_{calcd} (mg/m^3)	1.566
F(000)	4792
θ_{min}, θ_{max}, °	2.183, 19.999
R_1^a, wR_2^b ($I > 2\sigma(I)$)	0.0493, 0.0938
R_1^a, wR_2^b (all data)	0.0567, 0.0967

$^aR_1 = 3||F_o|-|F_c||/3|F_o|$. $^bwR_2 = [3[w(F_o^2 - F_c^2)^2]/3[w(F_o^2)^2]]^{½}$, $w = 1/\sigma^2(F_o^2) + (aP)^2 + bP$, where $P = [\max(0 \text{ or } F_o^2) + 2(F_c^2)]/3$.

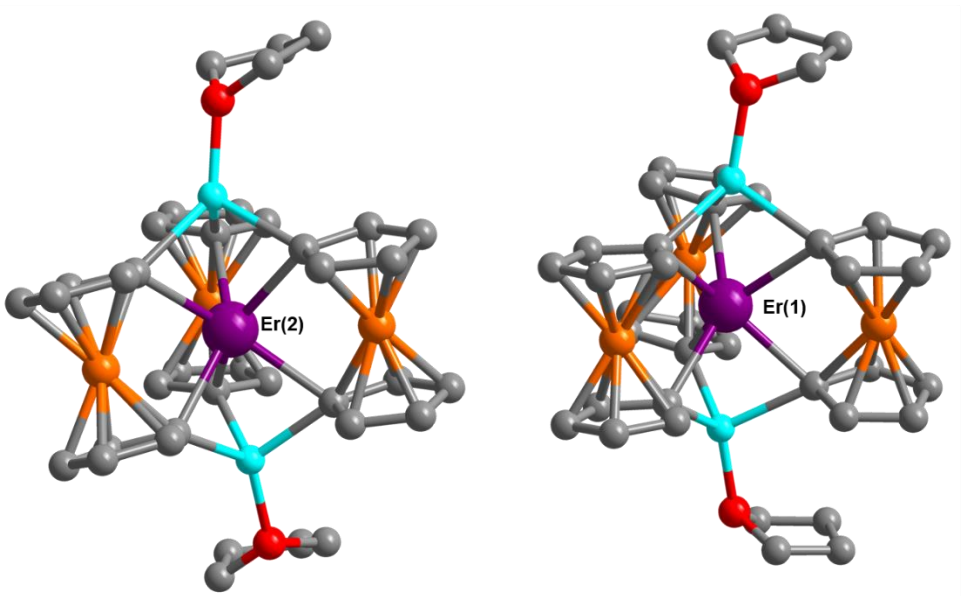

Fig. S5. Molecular structure of two independent molecules of monoanionic **3**. Atom labels are purple = Er, orange = Fe, light blue = Li, red = O, and grey = C. Hydrogen atoms and counter cations removed for clarity.

Table S6. Crystallographic Data for $[Li(THF)_4][TmFc_3(THF)_2Li_2]$ **(4)**.

Compound	**$\{Tm[(C_5H_4)_2Fe]_3[Li(THF)]_2\}\cdot Li(THF)_4$**
Formula	$C_{54}H_{72}TmFe_3Li_3O_6$
Crystal system	monoclinic
Space group	$P2_1/c$
a, Å	11.4199(15)
b, Å	63.606(8)
c, Å	13.7467
α,°	90
β,°	92.280(3)
γ, °	90
Volume, $Å^3$	9977(2)
Z	8
T, K	120
ρ_{calcd} (mg/m^3)	1.564
F(000)	4800
θ_{min}, θ_{max}, °	2.182, 25.000
R_1^a, wR_2^b ($I > 2\sigma(I)$)	0.0400, 0.0919
R_1^a, wR_2^b (all data)	0.0404, 0.0920

$^aR_1 = 3||F_o|-|F_c||/3|F_o|$. $^bwR_2 = [3[w(F_o^2 - F_c^2)^2]/3[w(F_o^2)^2]]^{½}$, $w = 1/\sigma^2(F_o^2) + (aP)^2 + bP$, where $P = [\max(0 \text{ or } F_o^2) + 2(F_c^2)]/3$.

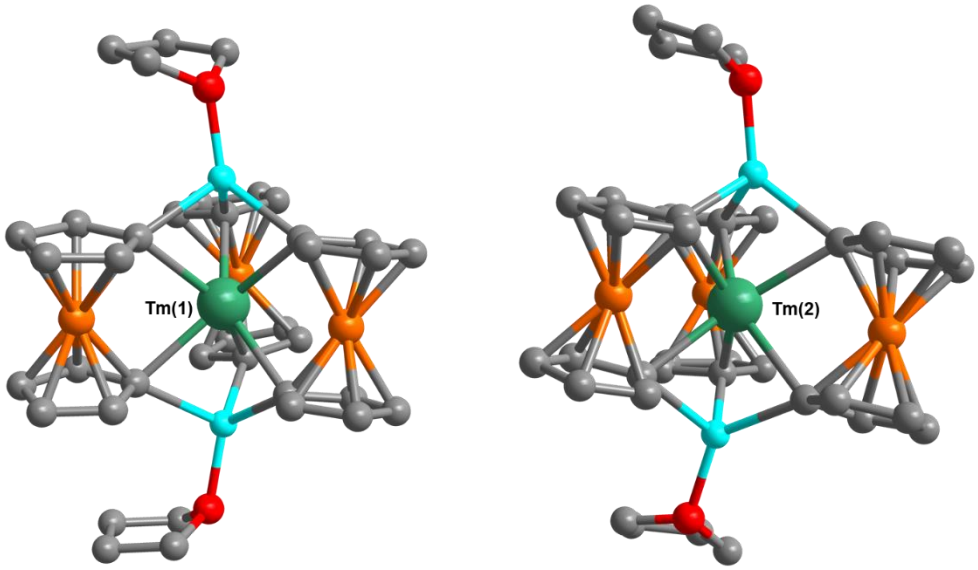

Fig. S6. Molecular structure of two independent molecules of monoanionic **4**. Atom labels are green = Tm, orange = Fe, light blue = Li, red = O, and grey = C. Hydrogen atoms and counter cations removed for clarity.

Table S7. Crystallographic Data for $[Li(THF)_4][YbFc_3(THF)_2Li_2]$ **(5)**.

Compound	**$\{Yb[(C_5H_4)_2Fe]_3[Li(THF)]_2\}\cdot Li(THF)_4$**
Formula	$C_{54}H_{72}YbFe_3Li_3O_6$
Crystal system	monoclinic
Space group	$P2_1/c$
a, Å	11.4155(6)
b, Å	63.489(3)
c, Å	13.7300(7)
α,°	90
β,°	92.170(2)
γ, °	90
Volume, $Å^3$	9943.9(9)
Z	8
T, K	110.0
ρ_{calcd} (mg/m^3)	1.574
F(000)	4808
θ_{min}, θ_{max}, °	2.199, 20.000
$R_1{}^a$, $wR_2{}^b$ (I > 2σ(I))	0.0774, 0.1571
$R_1{}^a$, $wR_2{}^b$ (all data)	0.0862, 0.1617

$^aR_1 = 3||F_o|-|F_c||/3|F_o|$. $^bwR_2 = [3[w(F_o^2 - F_c^2)^2]/3[w(F_o^2)^2]]^{½}$, $w = 1/\sigma^2(F_o^2) + (aP)^2 + bP$, where $P = [\max(0 \text{ or } F_o^2) + 2(F_c^2)]/3$.

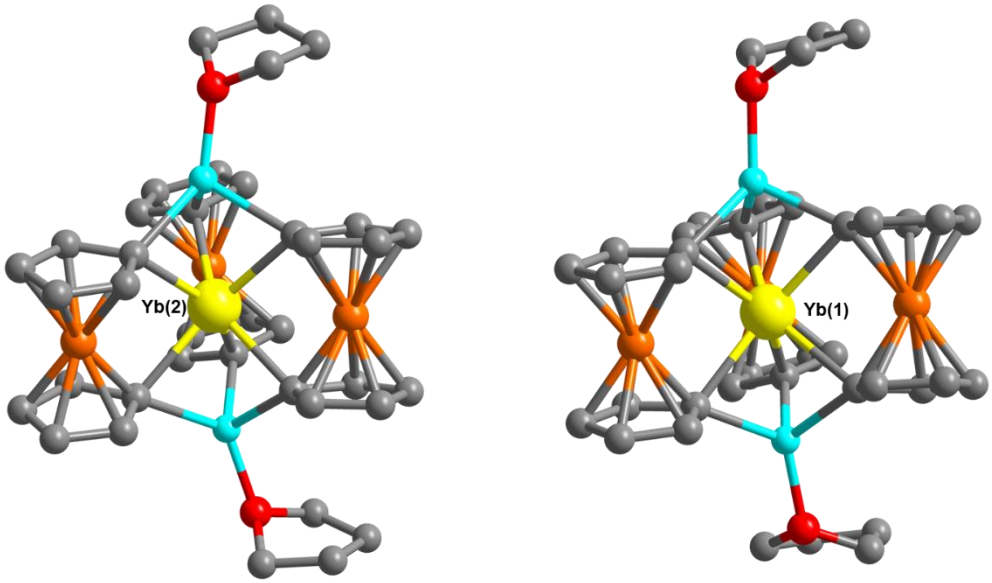

Fig. S7. Molecular structure of two independent molecules of monoanionic **5**. Atom labels are yellow = Yb, orange = Fe, light blue = Li, red = O, and grey = C. Hydrogen atoms and counter cations removed for clarity.

Table S8. Crystallographic Data for $[Li(THF)_4][YbFc_3(THF)_2Li_2]$ **(5^{Iso})**.

Compound	**$\{Yb[(C_5H_4)_2Fe]_3[Li(THF)]_2\}\cdot Li(THF)_4$**
Formula	$C_{54}H_{72}YbFe_3Li_3O_6 \cdot C_4H_8O$
Crystal system	monoclinic
Space group	Cc
a, Å	28.077(3)
b, Å	32.756(4)
c, Å	20.619(2)
α,°	90
β,°	120.475(2)°
γ, °	90
Volume, Å^3	16344(3)
Z	12
T, K	110.0
ρ_{calcd} (mg/m^3)	1.525
F(000)	7692
θ_{min}, θ_{max}, °	2.093, 27.500
R_1^a, wR_2^b (I > 2σ(I))	0.0414, 0.0963
R_1^a, wR_2^b (all data)	0.0485, 0.1054

$^aR_1 = 3||F_o|-|F_c||/3|F_o|$. $^bwR_2 = [3[w(F_o^2 - F_c^2)^2]/3[w(F_o^2)^2]]^{½}$, $w = 1/\sigma^2(F_o^2) + (aP)^2 + bP$, where $P = [\max(0 \text{ or } F_o^2) + 2(F_c^2)]/3$.

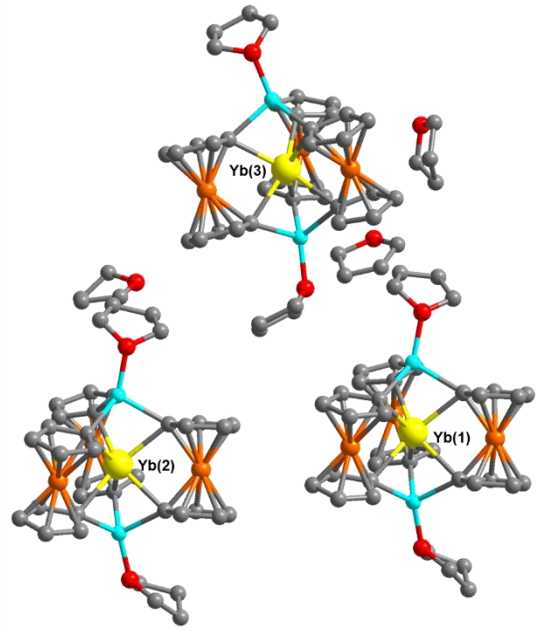

Fig. S8. Molecular structure of three independent molecules of monoanionic **5^{Iso}** and THF lattice solvate molecules. Atom labels are yellow = Yb, orange = Fe, light blue = Li, red = O, and grey = C. Hydrogen atoms and counter cations removed for clarity.

Table S9. Crystallographic Data for $[Li(THF)_4][LuFc_3(THF)_2Li_2]$ **(6)**.

Compound	**$\{Lu[(C_5H_4)_2Fe]_3[Li(THF)]_2\}\cdot Li(THF)_4$**
Formula	$C_{54}H_{72}LuFe_3Li_3O_6$
Crystal system	monoclinic
Space group	$P2_1/c$
a, Å	11.4149(16)
b, Å	63.246(9)
c, Å	13.7430(19)
α,°	90
β,°	92.282(4)
γ, °	90
Volume, $Å^3$	9914(2)
Z	8
T, K	110.0
ρ_{calcd} (mg/m^3)	1.582
F(000)	4816
θ_{min}, θ_{max}, °	2.189, 25.000
R_1^a, wR_2^b ($I > 2\sigma(I)$)	0.0666, 0.1537
R_1^a, wR_2^b (all data)	0.0749, 0.1603

$^aR_1 = 3||F_o|-|F_c||/3|F_o|$. $^bwR_2 = [3[w(F_o^2 - F_c^2)^2]/3[w(F_o^2)^2]]^{½}$, $w = 1/\sigma^2(F_o^2) + (aP)^2 + bP$, where $P = [\max(0 \text{ or } F_o^2) + 2(F_c^2)]/3$.

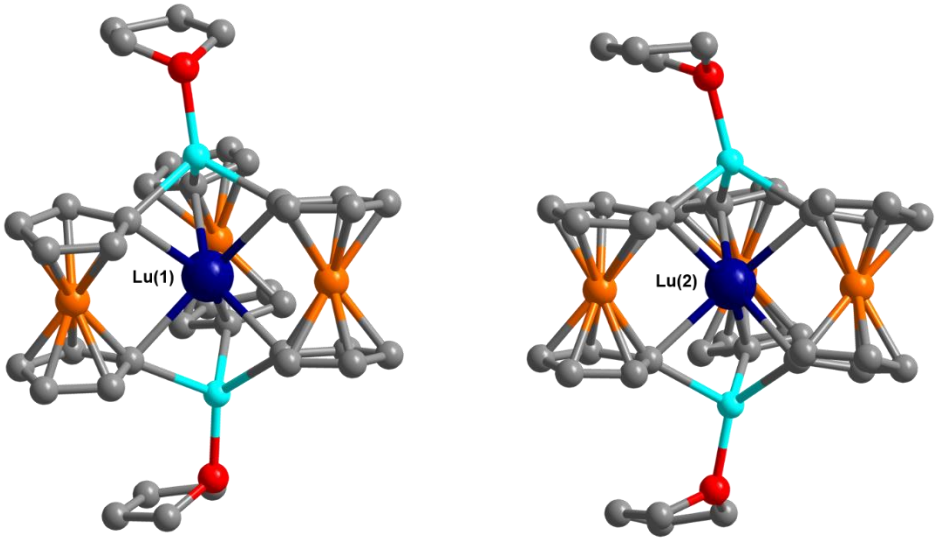

Fig. S9. Molecular structure of two independent molecules of monoanionic **6**. Atom labels are navy = Lu, orange = Fe, light blue = Li, red = O, and grey = C. Hydrogen atoms and counter cations removed for clarity.

Table S10. Crystallographic Data for $[Li(THF)_4][LuFc_3(THF)_2Li_2]$ **(6^{Iso})**.

Compound	**$\{Lu[(C_5H_4)_2Fe]_3[Li(THF)]_2\}\cdot Li(THF)_4$**
Formula	$C_{54}H_{72}LuFe_3Li_3O_6 \cdot C_4H_8O$
Crystal system	monoclinic
Space group	I_a
a, Å	20.620(3)
b, Å	32.856(4)
c, Å	25.081(4)
α,°	90
β,°	104.923(10)
γ, °	90
Volume, Å^3	16419(4)
Z	12
T, K	120.0
ρ_{calcd} (mg/m^3)	1.520
F(000)	7704
θ_{min}, θ_{max}, °	2.041, 34.356
R_1[a], wR_2[b] (I > 2σ(I))	0.0876, 0.2237
R_1[a], wR_2[b] (all data)	0.1014, 0.2475

[a]$R_1 = 3||F_o|-|F_c||/3|F_o|$. [b]$wR_2 = [3[w(F_o^2 - F_c^2)^2]/3[w(F_o^2)^2]]^{½}$, $w = 1/\sigma^2(F_o^2) + (aP)^2 + bP$, where $P = [\max(0 \text{ or } F_o^2) + 2(F_c^2)]/3$.

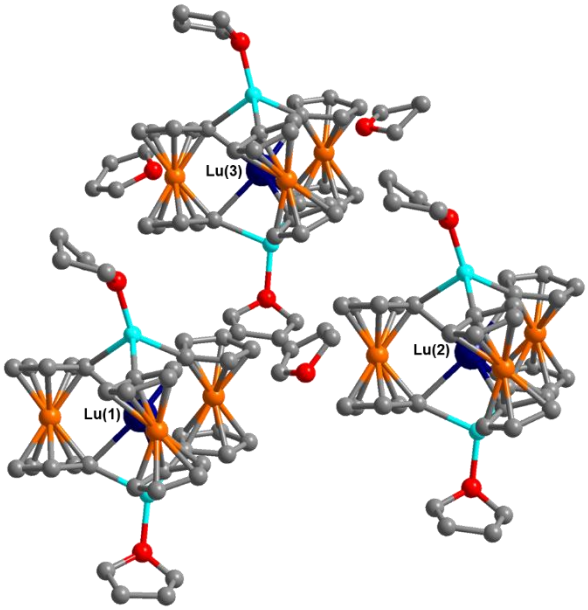

Fig. S10. Molecular structure of three independent molecules of monoanionic **6^{Iso}** and THF lattice solvate molecules. Atom labels are navy = Lu, orange = Fe, light blue = Li, red = O, and grey = C. Hydrogen atoms and counter cations removed for clarity.

Table S11. Selected distances and angles in the molecular structure of **1-6**.

Selected Interatomic Distances and Angles						
Compound	**1 (Gd)**	**2 (Ho)**	**3 (Er)**	**4 (Tm)**	**5 (Yb)**	**6 (Lu)**
Ln(1)-C, Å	2.566(9)	2.520(13)	2.525(9)	2.515(5)	2.474(17)	2.489(11)
Average	2.576(8)	2.524(12)	2.512(10)	2.539(5)	2.447(17)	2.513(10)
	2.564(8)	2.538(14)	2.513(9)	2.521(5)	2.520(16)	2.482(11)
	2.579(8)	2.531(13)	2.515(9)	2.504(5)	2.503(16)	2.517(10)
	2.582(8)	2.555(13)	2.507(10)	2.529(5)	2.503(17)	2.492(11)
	2.563(8)	2.523(13)	2.552(9)	2.513(5)	2.548(16)	2.511(11)
	2.572[8]	**2.532[13]**	**2.521[9]**	**2.520[5]**	**2.499[17]**	**2.501[11]**
Ln(2)-C, Å	2.568(8)	2.512(12)	2.500(9)	2.509(5)	2.501(16)	2.501(11)
Average	2.583(8)	2.543(13)	2.525(9)	2.515(5)	2.478(16)	2.497(10)
	2.555(8)	2.536(13)	2.538(9)	2.519(5)	2.501(16)	2.489(11)
	2.581(8)	2.547(12)	2.518(9)	2.509(5)	2.517(16)	2.505(11)
	2.561(8)	2.528(12)	2.539(9)	2.533(5)	2.524(16)	2.511(10)
	2.564(9)	2.569(12)	2.514(10)	2.518(5)	2.495(17)	2.481(10)
	2.569[8]	**2.539[12]**	**2.522[9]**	**2.517[5]**	**2.503[16]**	**2.497[11]**
Ln(1)···Fe, Å	3.1953(12)	3.1846(19)	3.1844(14)	3.2538(8)	3.177(2)	3.2531(16)
	3.2201(12)	3.212(2)	3.2137(14)	3.1806(8)	3.208(2)	3.1736(15)
Average	3.2688(12)	3.263(2)	3.2606(14)	3.2083(8)	3.253(2)	3.2057(16)
	3.2281[12]	**3.229[8]**	**3.2196[14]**	**3.214[8]**	**3.213[2]**	**3.2108[16]**
Ln(2)···Fe, Å	3.2187(12)	3.2202(19)	3.2251(14)	3.2169(8)	3.220(2)	3.1944(16)
	3.2306(12)	3.234(2)	3.2024(13)	3.2193(8)	3.212(2)	3.2085(16)
Average	3.2408(12)	3.2078(19)	3.2241(14)	3.1988(8)	3.195(2)	3.2176(15)
	3.2300[12]	**3.221[13]**	**3.2172[14]**	**3.212[8]**	**3.209[2]**	**3.2068[16]**
C1-Fe-C1 For Ln(1)	106.6(3)	104.4(5)	104.3(4)	101.8(2)	101.5(7)	100.4(4)
	105.6(3)	103.9(5)	102.7(4)	104.1(2)	103.0(7)	103.7(4)
	103.6(3)	102.1(5)	101.7(4)	103.4(2)	101.8(7)	102.4(4)
	105.3[3]	**103.5[5]**	**102.9[4]**	**103.1[2]**	**102.1[7]**	**102.2[4]**
C1-Fe-C1 For Ln(2)	105.7(3)	103.2(5)	102.2(4)	102.5(2)	101.1(7)	102.7(4)
	104.9(3)	103.4(5)	104.0(4)	102.6(2)	102.5(7)	102.0(4)
	104.2(3)	104.8(5)	103.0(4)	103.9(2)	103.3(6)	101.7(4)
	104.9[3]	**103.8[5]**	**103.1[4]**	**103.0[2]**	**102.3[7]**	**102.1[1]**
C-Ln(1)-C (°)	82.0(3)	82.4(4)	81.6(3)	79.8(2)	81.3(6)	79.8(3)
	81.0(3)	81.2(4)	80.8(3)	81.9(2)	81.0(6)	81.8(3)
Average	79.7(3)	80.2(4)	79.7(3)	81.0(2)	80.6(6)	80.7(4)
	80.9[3]	**81.3[4]**	**80.7[3]**	**80.9[2]**	**81.0[6]**	**80.8[4]**
C-Ln(2)-C (°)	81.4(3)	81.5(4)	80.2(3)	80.5(2)	81.7(6)	81.6(3)
	81.6(2)	81.0(4)	81.2(3)	81.0(2)	80.1(6)	81.0(4)
Average	79.9(3)	81.5(4)	80.9(3)	81.5(2)	81.5(5)	80.8(4)
	81.0[3]	**81.3[4]**	**80.8[3]**	**81.0[2]**	**81.1[6]**	**81.1[4]**

Ln(1) Fc^{2-} Twist (°) **|Average|** **|Range|**	**8.16** Min: **7.42** Max: **9.31**	**10.67** Min: **10.37** Max: **11.16**	**11.57** Min: **11.39** Max: **11.75**	**12.76** Min: **12.47** Max: **13.22**	**13.18** Min: **12.68** Max: **13.49**	**14.24** Min: **14.11** Max: **14.46**
Ln(2) Fc^{2-} Twist (°) **|Average|** **|Range|**	**9.64** Min: **9.36** Max: **10.00**	**12.67** Min: **12.09** Max: **13.58**	**14.49** Min: **13.89** Max: **15.32**	**16.23** Min: **15.60** Max: **17.21**	**16.65** Min: **16.31** Max: **17.13**	**18.56** Min: **17.67** Max: **19.69**

Table S12. Selected distances and angles in the molecular structure of **5^{Iso} and 6^{Iso}**.

Selected Interatomic Distances and Angles				
Compound	**5**	**5^{Iso}**	**6**	**6^{Iso}**
Ln-C, Å **Average**	Ln(1): **2.499[17]** Ln(2): **2.503[16]**	Ln(1): **2.499[8]** Ln(2): **2.492[7]** Ln(3): **2.493[7]**	Ln(1): **2.501[11]** Ln(2): **2.497[11]**	Ln(1): **2.494[9]** Ln(2): **2.494[8]** Ln(3): **2.488[9]**
Ln···Fe, Å **Average**	Ln(1): **3.213[2]** Ln(2): **3.209[2]**	Ln(1): **3.2167[11]** Ln(2): **3.1899[11]** Ln(3): **3.1916[11]**	Ln(1): **3.2108[16]** Ln(2): **3.2068[16]**	Ln(1): **3.2103 [13]** Ln(2): **3.1945 [13]** Ln(3): **3.1962 [13]**
C-Ln-C (°) **Average**	Ln(1): **81.0[6]** Ln(2): **81.1[6]**	Ln(1): **80.9[3]** Ln(2): **81.4[3]** Ln(3): **81.4[3]**	Ln(1): **80.8[4]** Ln(2): **81.1[4]**	Ln(1): **80.7[2]** Ln(2): **81.3[3]** Ln(3): **81.3[3]**
Ln Fc^{2-} Twist (°) **|Average|**	Ln(1): **13.21** Ln(2): **16.62**	Ln(1): **16.33** Ln(2): **19.77** Ln(3): **19.88**	Ln(1): **14.25** Ln(2): **18.55**	Ln(1): **17.35** Ln(2): **20.81** Ln(3): **20.92**

Table S13. Selected distances and angles in the molecular structure of **2-py** and **2-THF***.

Selected Interatomic Distances and Angles			
Compound	**2**	**2-py**	**2-THF***
Ln(1)-C, Å **Average**	**2.532[13]**	2.512(13) 2.530(13) 2.520(12) 2.512(13) 2.526(13) 2.523(13) **2.521[13]**	2.554(8) 2.522(9) 2.530(8) 2.540(9) 2.527(8) 2.546(9) **2.537[9]**
Ln(2)-C, Å **Average**	**2.539[12]**	2.517(12) 2.512(12) 2.532(12) 2.504(12) 2.506(13) 2.528(12) **2.517[12]**	
Ln(1)···Fe, Å **Average**	**3.229[8]**	3.1837(15) 3.2187(15) 3.1885(16) **3.1970[15]**	3.2180(12) 3.1978(13) 3.2136(13) **3.2098[13]**
Ln(2)···Fe, Å **Average**	**3.221[13]**	3.1768(16) 3.1454(16) 3.1630(16) **3.1617[16]**	
C-Ln(1)-C (°) **Average**	**80.9[3]**	82.0(5) 80.8(4) 82.2(4) **81.7[4]**	80.4(3) 81.4(3) 81.2(3) **81.0[3]**
C-Ln(2)-C (°) **Average**	**81.0[3]**	81.9(4) 82.8(4) 82.7(4) **82.5[4]**	
Ln(1) Fc^{2-} Twist (°) **|Average|** **|Range|**	**10.64** Min: **10.37** Max: **11.16**	**19.24** Min: **17.85** Max: **21.45**	**16.52** Min: **15.11** Max: **17.68**
Ln(2) Fc^{2-} Twist (°) **|Average|** **|Range|**	**12.67** Min: **12.09** Max: **13.58**	**23.69** Min: **22.95** Max: **24.40**	

Table S14. The closest intermolecular distances in **2**, **2-py**, and **2-THF***.

Closest Intermolecular Distance Between Ho(III) Ions, Å		
2 (Ho(2)-Ho(2))	**2-py (Ho(1)-Ho(2))**	**2-THF***
10.586	8.941	11.069

Magnetism:

Static Magnetic Properties

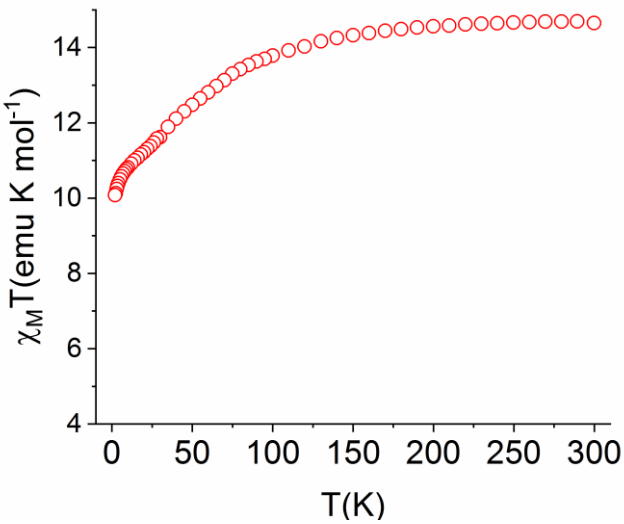

Fig. S11. Temperature dependence of the molar magnetic susceptibility temperature product ($\chi_M T$) of **2-py**, where H = 0.1 T and T = 300 K – 2K.

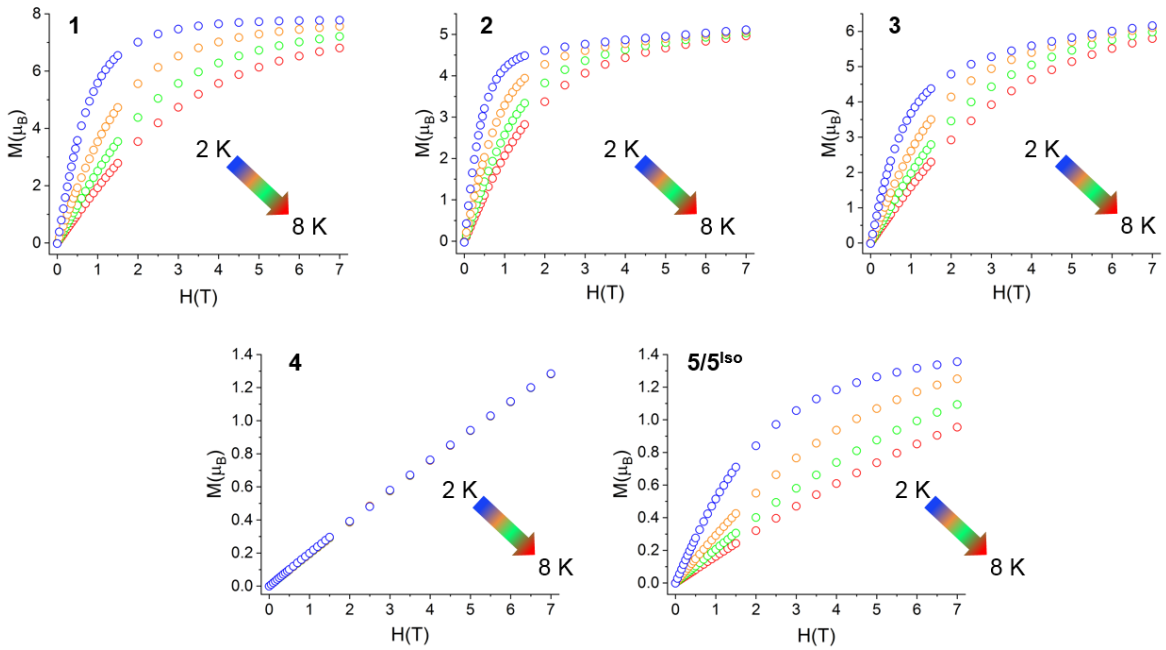

Fig. S12. M vs. H curves of **1-5/5^{Iso}** where H = 0 – 7 T and T = 8 K – 2K.

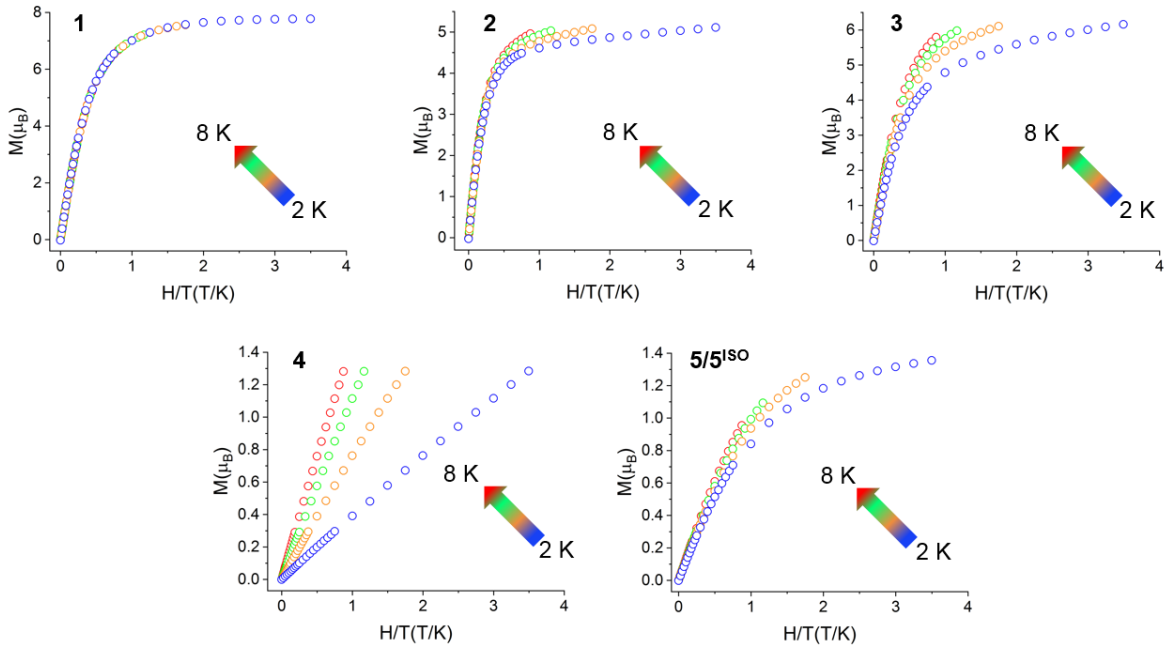

Fig. S13. M vs. H/T curves of **1-5/5^{Iso}** where H = 0 – 7 T and T = 8 K – 2K.

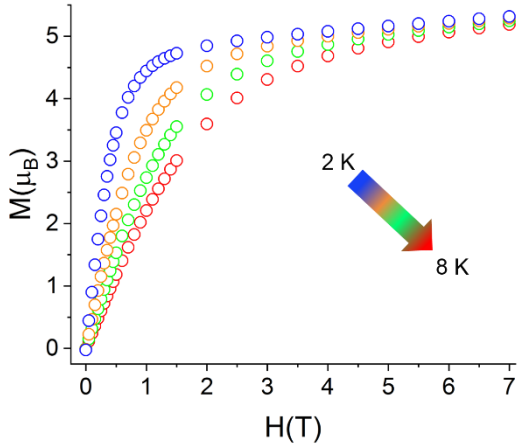

Fig. S14. M vs. H curves of **2-py** where H = 0 – 7 T and T = 8 K – 2K.

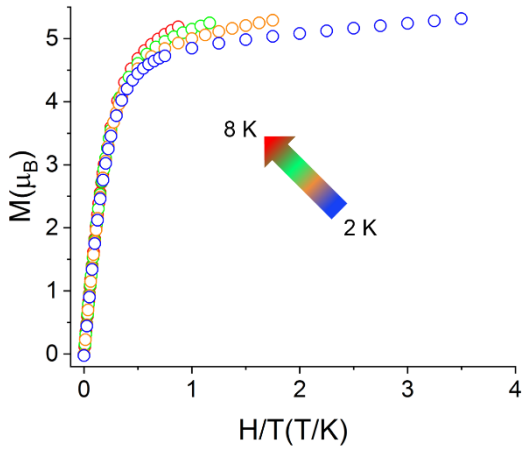

Fig. S15. M vs. H/T curves of **2-py**, where H = 0 – 7 T and T = 8 K – 2K.

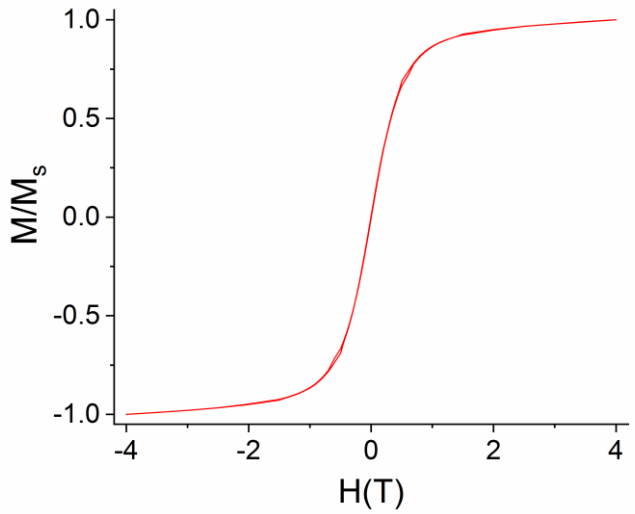

Fig. S16. M vs. H curve of **2** where H = 0 – 4 T and T = 2 K.

Dynamic Magnetic Properties

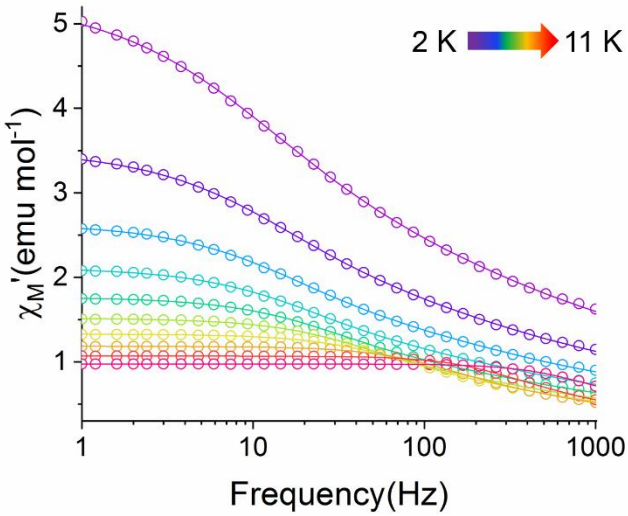

Fig. S17. Temperature dependence of the in-phase component of the molar ac magnetic susceptibility (χ_M') of **2** where H = 0 T and T = 2- 11 K. Lines represent fits to experimental data (solid circles).

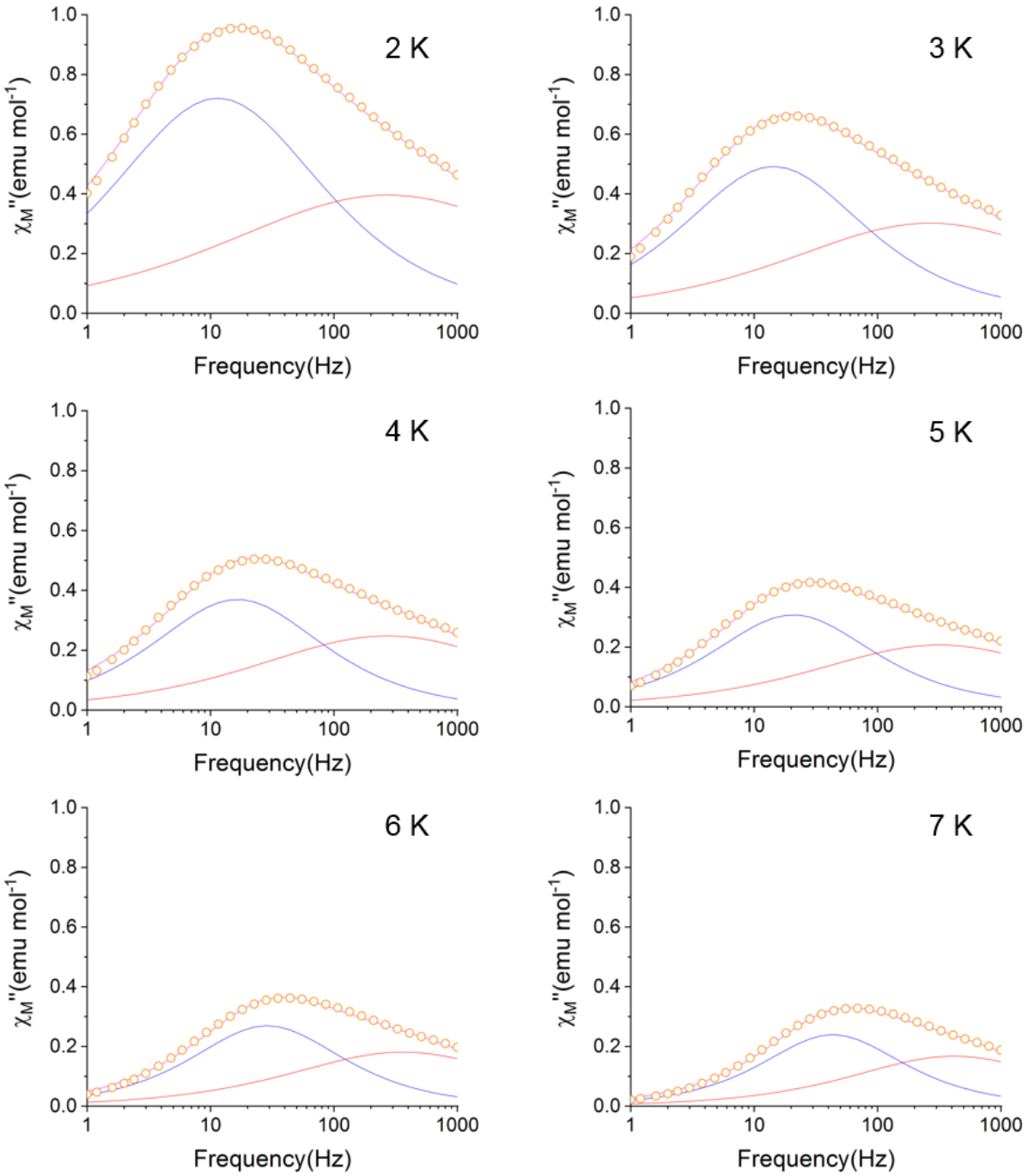

Fig. S18. Frequency dependence of the resolved components of the out-of-phase component of the ac magnetic susceptibility (χ_M'') between 2 K – 7 K for **2**. Orange circles represent experiment data and lines represent full fit (violet) and resolved fast (red) and slow (blue) relaxation processes.

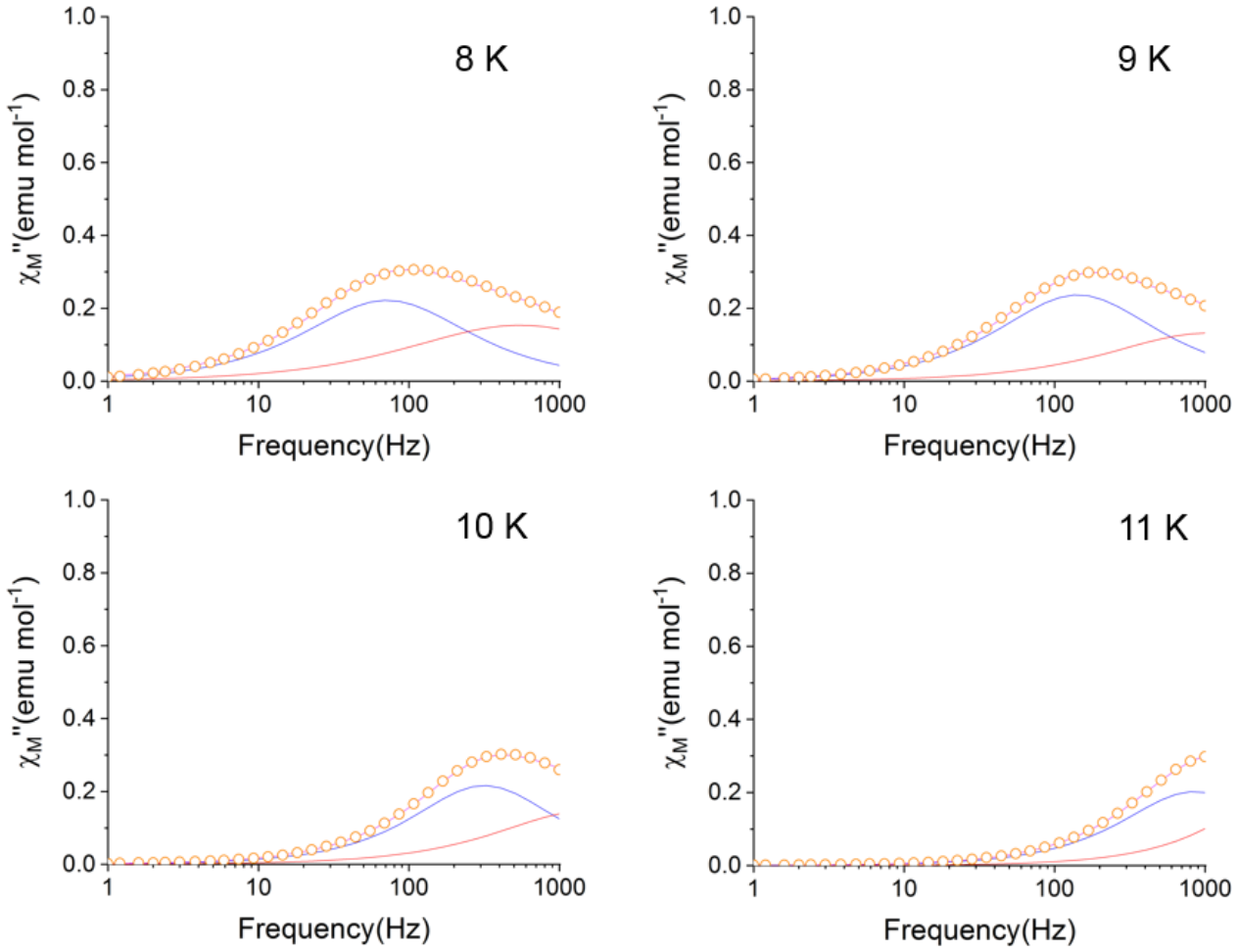

Fig. S19. Frequency dependence of the resolved components of the out-of-phase component of the ac magnetic susceptibility (χ_M'') between 8 K – 11 K for **2**. Orange circles represent experiment data and lines represent full fit (violet) and resolved fast (red) and slow (blue) relaxation processes.

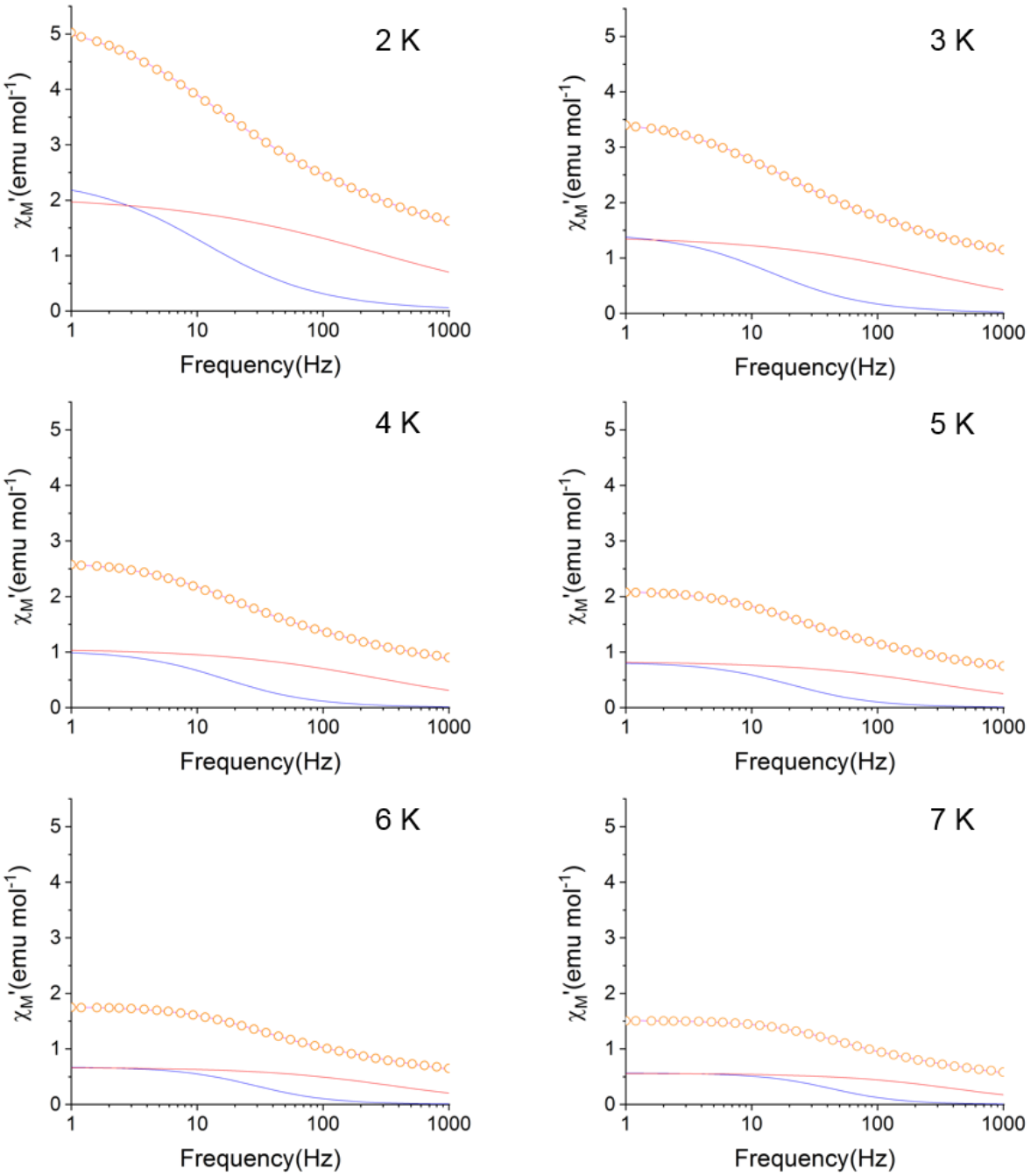

Fig. S20. Frequency dependence of the resolved components of the in-phase component of the ac magnetic susceptibility (χ_M') between 2 K – 7 K for **2**. Orange circles represent experiment data and lines represent full fit (violet) and resolved fast (red) and slow (blue) relaxation processes.

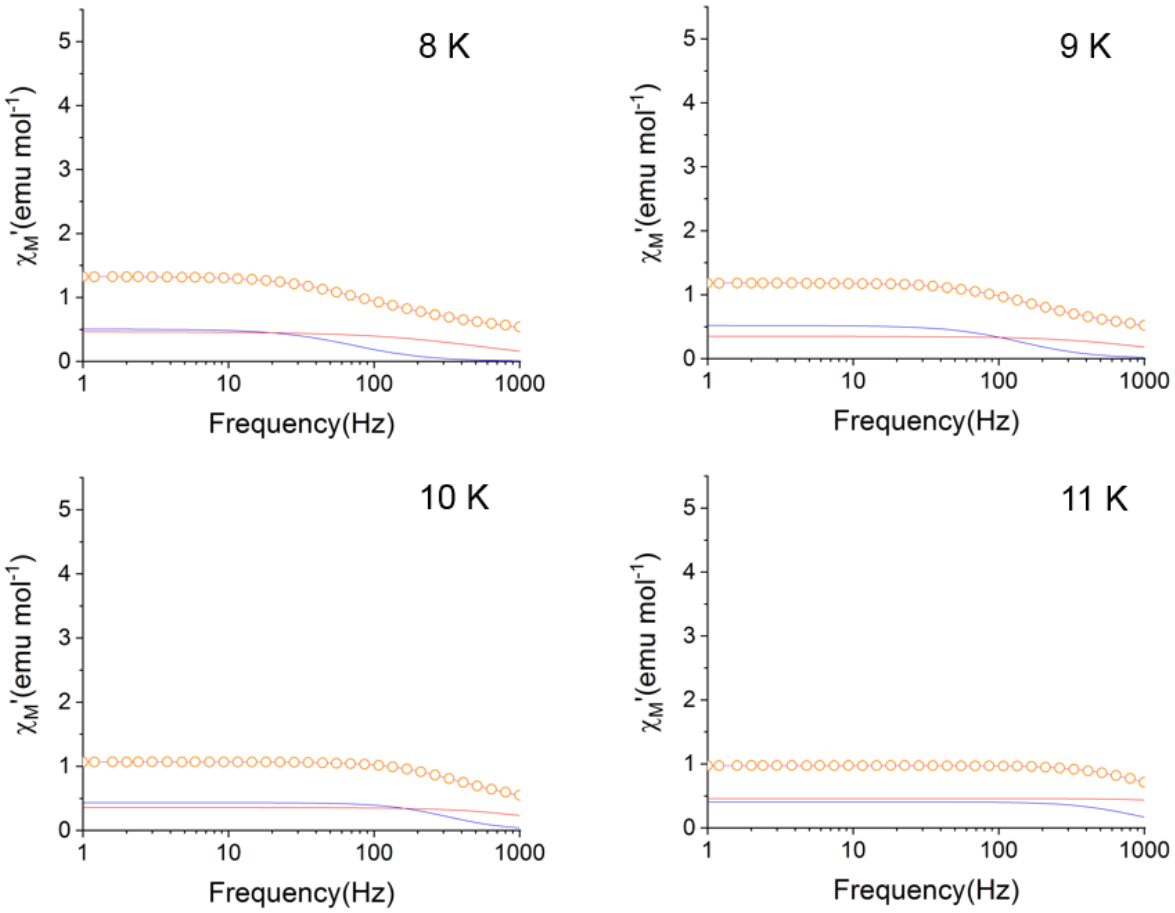

Fig. S21. Frequency dependence of the resolved components of the in-phase component of the ac magnetic susceptibility (χ_M') between 8 K – 11 K for **2**. Orange circles represent experiment data and lines represent full fit (violet) and resolved fast (red) and slow (blue) relaxation processes.

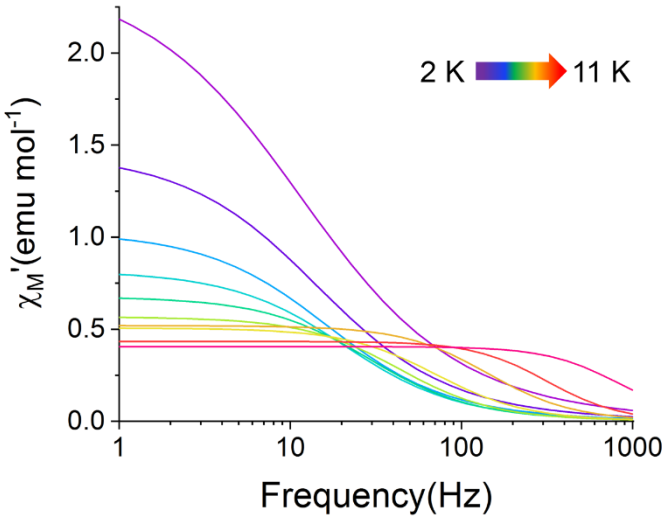

Fig. S22. Temperature dependence of resolved slow relaxation process **(SR)** of the in-phase component of the molar ac magnetic susceptibility (χ_M'') of **2** where H = 0 T and T = 2 - 11 K.

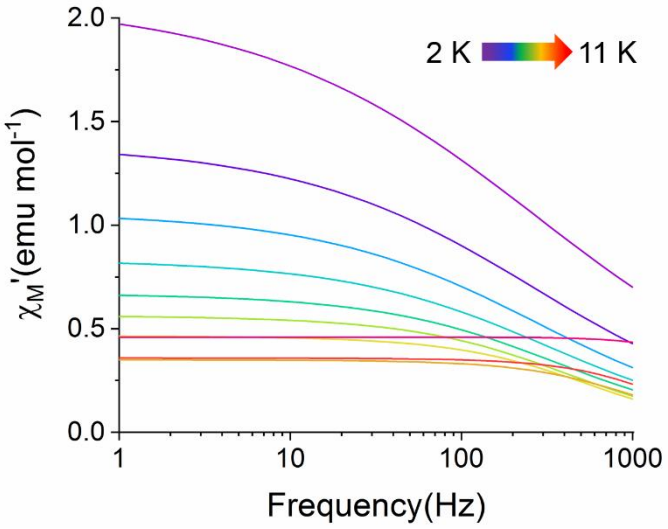

Fig. S23. Temperature dependence of resolved fast relaxation process **(FR)** of the in-phase component of the molar ac magnetic susceptibility (χ_M'') of **2** where H = 0 T and T = 2 - 11 K.

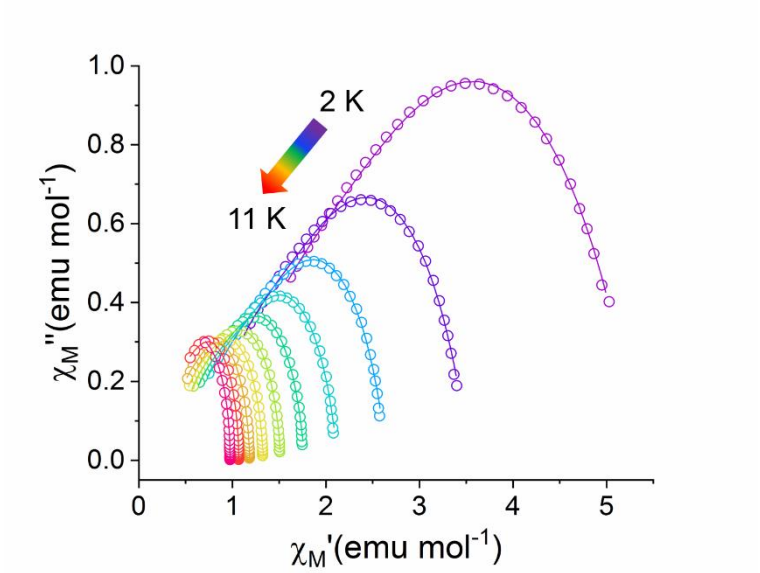

Fig. S24. Cole-Cole plot (χ_M''vs. χ_M') of **2** where H = 0 T and T = 2 – 11 K. Lines represent fits to experimental data (circles).

Table S15. Cole-Cole fitting parameters for **[HoFc$_3$(THF)$_2$Li$_2$]$^-$ (H = 0 T)**

T(K)	$\chi_{s,tot}$	$\Delta\chi_1$	τ_1	α_1	$\Delta\chi_2$	τ_2	α_2
2	0.837065	2.44042	0.01387	0.320696	2.08576	0.000581	0.537794
3	0.672596	1.46811	0.011056	0.248379	1.39345	0.000598	0.478818
4	0.555655	1.03506	0.009609	0.210351	1.06285	0.000586	0.444177
5	0.471506	0.821297	0.007663	0.180637	0.833489	0.000505	0.412631
6	0.423399	0.67896	0.005522	0.145687	0.670095	0.000439	0.369098
7	0.388803	0.567887	0.003664	0.107807	0.562929	0.000382	0.31671
8	0.359154	0.506863	0.002228	0.083516	0.465679	0.000291	0.25728
9	0.31528	0.519729	0.001115	0.058846	0.350163	0.000153	0.176574
10	0.276774	0.43338	0.000501	1.4E-07	0.358707	0.000104	0.127445
11	0.110725	0.405319	0.000188	4.35E-07	0.458762	0.0000368	0.001683

$\chi_{s,tot}$ = adiabatic susceptibilty
$\Delta\chi_1$ and **$\Delta\chi_2$ =** Difference between the adiabatic susceptibilty (χ_s) and isothemeral susceptibilty (χ_T) for relaxation process 1 and 2.
α_1 and α_2 = Magnetic relaxation time distribution parameter for relaxation process 1 and 2.
τ_1 and τ_2 = Magnetic relaxation times for relaxation process 1 and 2.

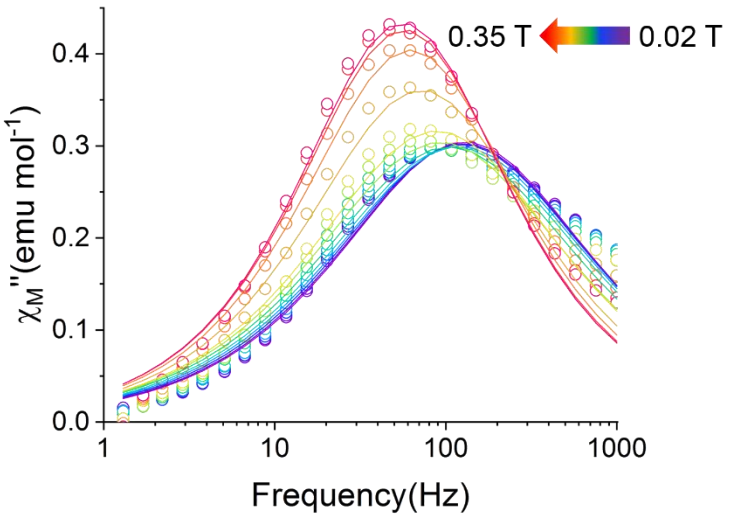

Fig. S25. Field dependence of the out-of-phase component of the molar ac magnetic susceptibility (χ_M'') of **2** where H = 0.02 T – 0.35 T and T = 8 K. Lines represent fits to experimental data (circles).

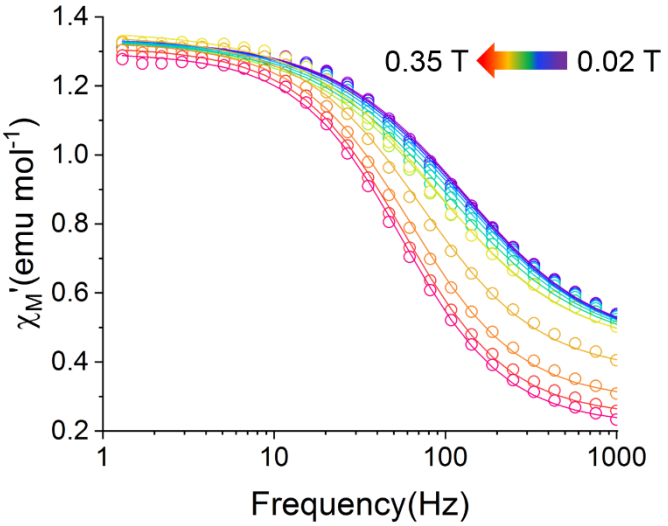

Fig. S26. Field dependence of the in-phase component of the molar ac magnetic susceptibility (χ_M') of **2** where H = 0.02 T – 0.35 T and T = 8 K. Lines represent fits to experimental data (circles).

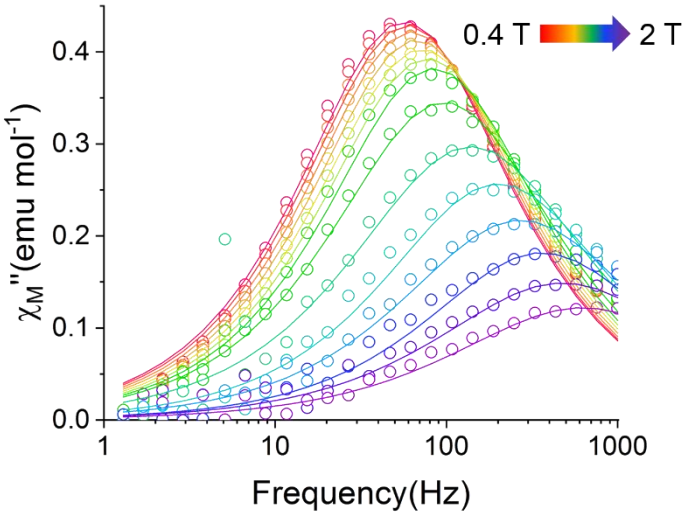

Fig. S27. Field dependence of the out-of-phase component of the molar ac magnetic susceptibility (χ_M'') of **2** where H = 0.4 T – 2 T and T = 8 K. Lines represent fits to experimental data (circles).

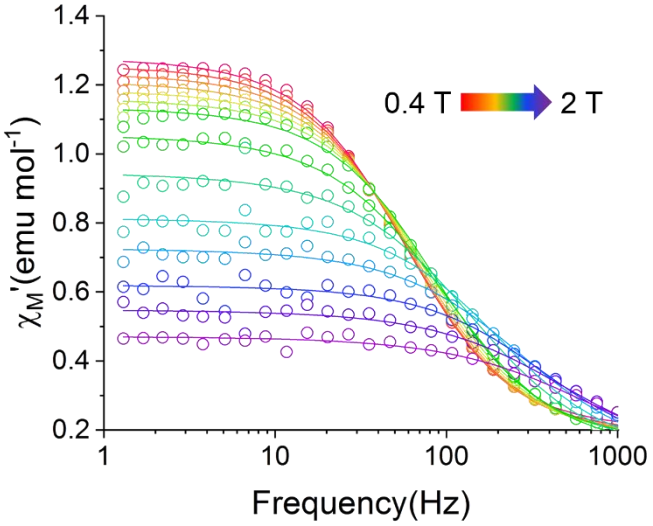

Fig. S28. Field dependence of the in-phase component of the molar ac magnetic susceptibility (χ_M') of **2** where H = 0.4 T – 2 T and T = 8 K. Lines represent fits to experimental data (circles).

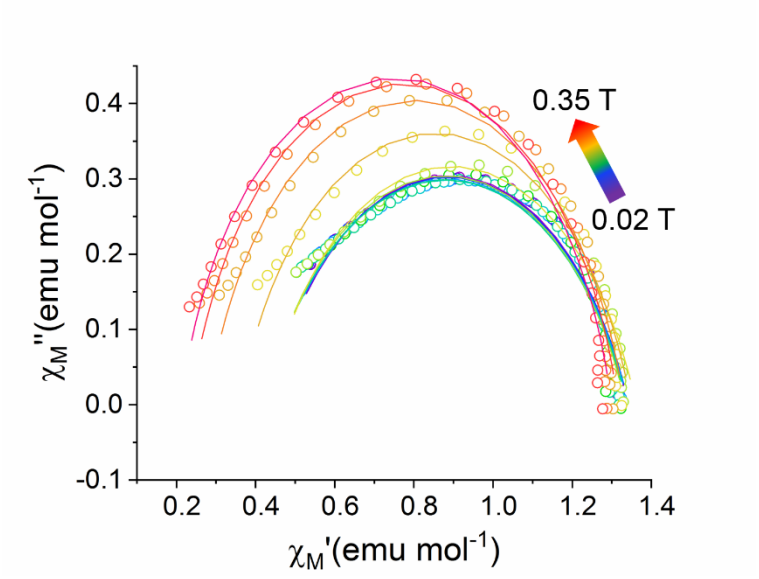

Fig. S29. Cole-Cole plot (χ_M'' vs. χ_M') of **2** where H = 0.02 T - 0.35 T and T = 8 K. Lines represent fits to experimental data (circles).

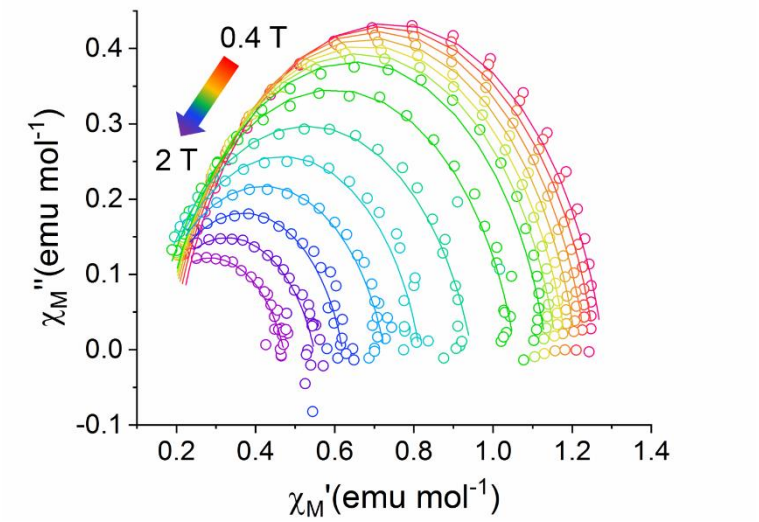

Fig. S30. Cole-Cole plot (χ_M'' vs. χ_M') of **2** where H = 0.4 T - 2 T and T = 8 K. Lines represent fits to experimental data (circles).

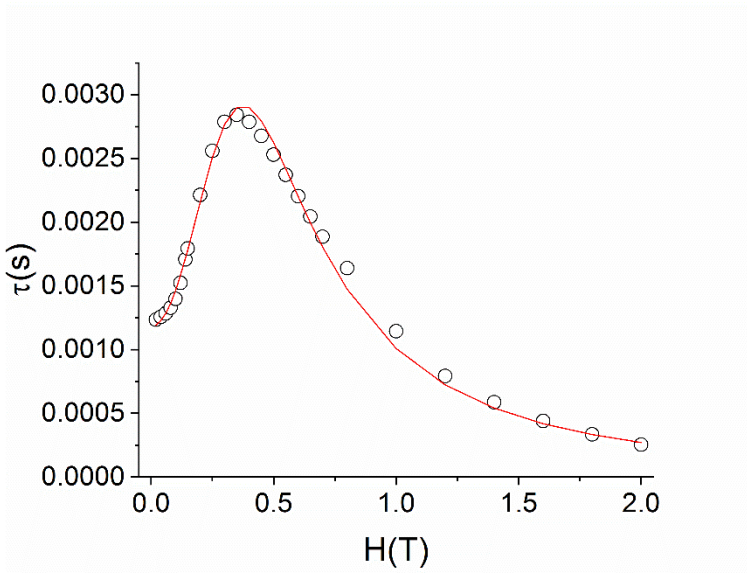

Fig. S31. Plot of the magnetic relaxation time vs. field (τ vs. H) of **2** where T = 8 K and H = 0 – 2 T. Line represents fit to the experimental data (circles). Data modeled using $\tau^{-1} = AH^2T + (B_1)/(1+B_2H^2) + D$.

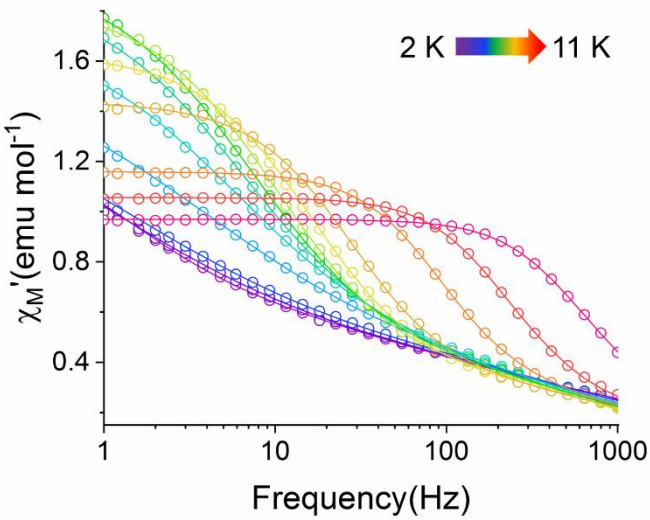

Fig. S32. Temperature dependence of the in-phase component of the molar ac magnetic susceptibility (χ_M') of **2** where H = 0.35 T and T = 2 – 11 K. Lines represent fits to the experimental data (circles).

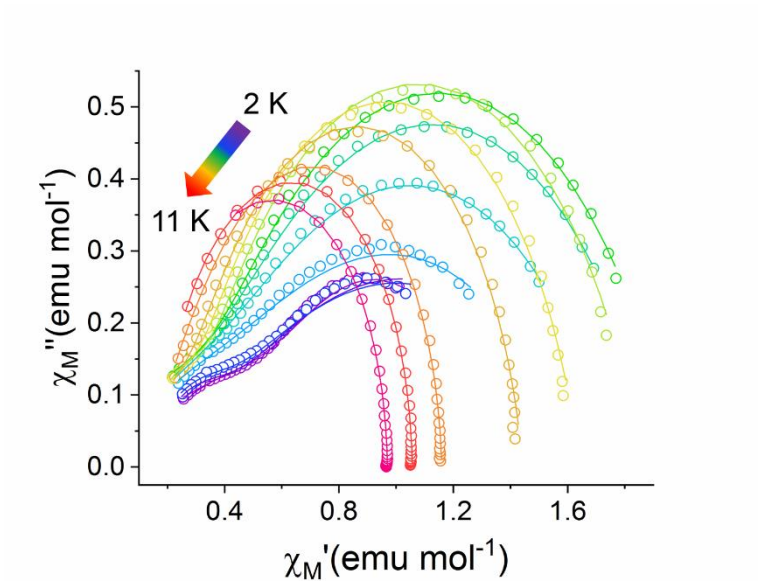

Fig. S33. Cole-Cole plot (χ_M''vs. χ_M') of **2** where H = 0.35 T and T = 2 – 11 K. Lines represent fits to experimental data (solid circles).

Table S16. Cole-Cole fitting parameters for **[HoFc$_3$(THF)$_2$Li$_2$]$^-$ (H = 0.35 T)**

T(K)	$\chi_{s,tot}$	$\Delta\chi_1$	τ_1	α_1	$\Delta\chi_2$	τ_2	α_2
1.8	0.121267	1.10824	0.136228	0.452703	0.318101	0.000354	0.405668
1.9	0.129339	1.34716	0.16487	0.533196	0.226433	0.000296	0.305769
2	0.118247	1.31795	0.127375	0.535112	0.237446	0.000296	0.320223
2.5	1.53E-07	1.08145	0.048962	0.437682	0.550042	0.00044	0.583627
3	9.59E-15	1.22486	0.028732	0.340974	0.539796	0.000385	0.561675
3.5	1.33E-08	1.44315	0.025329	0.296937	0.475304	0.000254	0.525791
4	0.009325	1.58636	0.022038	0.27885	0.37512	0.000145	0.417131
5	0.125443	1.55112	0.015372	0.238237	0.18023	0.000214	0.067031
6	0.091146	1.322	0.009706	0.17691	0.226382	0.00016	0.221839
7	0.072171	1.09149	0.005769	0.120676	0.279607	0.000163	0.372363
9	0.150706	0.809643	0.001774	0.037495	0.199738	0.00027	0.18207
10	0.171263	0.536739	0.00082	0.001607	0.348674	0.000378	0.099377
11	0.130616	0.462177	0.000307	3.4E-11	0.376737	0.000135	0.083831

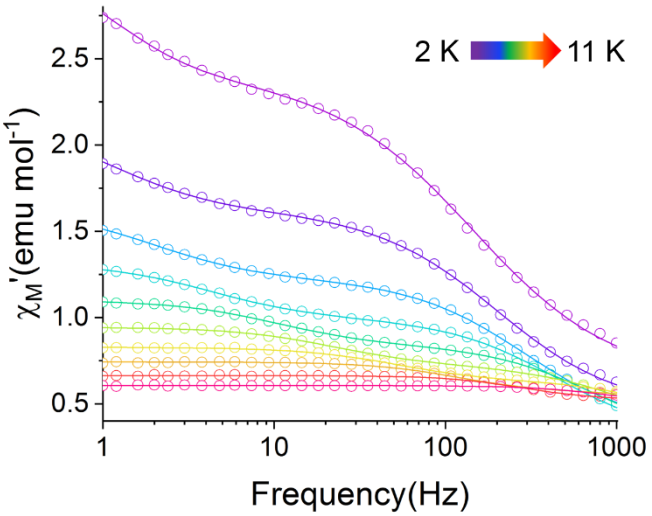

Fig. S34. Temperature dependence of the in-phase component of the molar ac magnetic susceptibility (χ_M') of **2-dilute** where H = 0 T and T = 2 – 11 K. Lines represent fits to experimental data (circles).

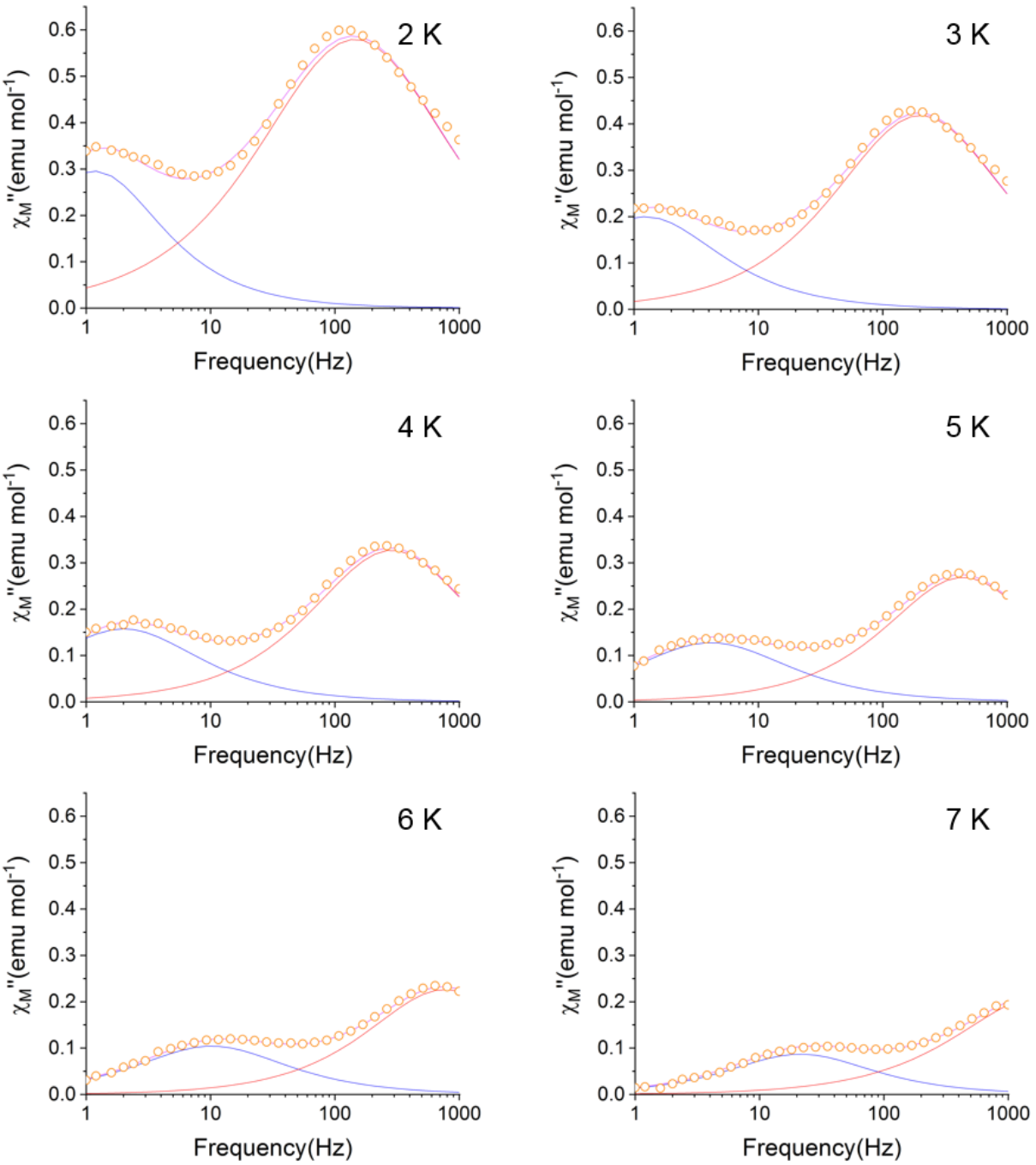

Fig. S35. Frequency dependence of the resolved components of the out-of-phase component of the ac magnetic susceptibility (χ_M'') between 2 K – 7 K for **2-dilute**. Orange circles represent experiment data and lines represent full fit (violet) and resolved fast (red) and slow (blue) relaxation processes.

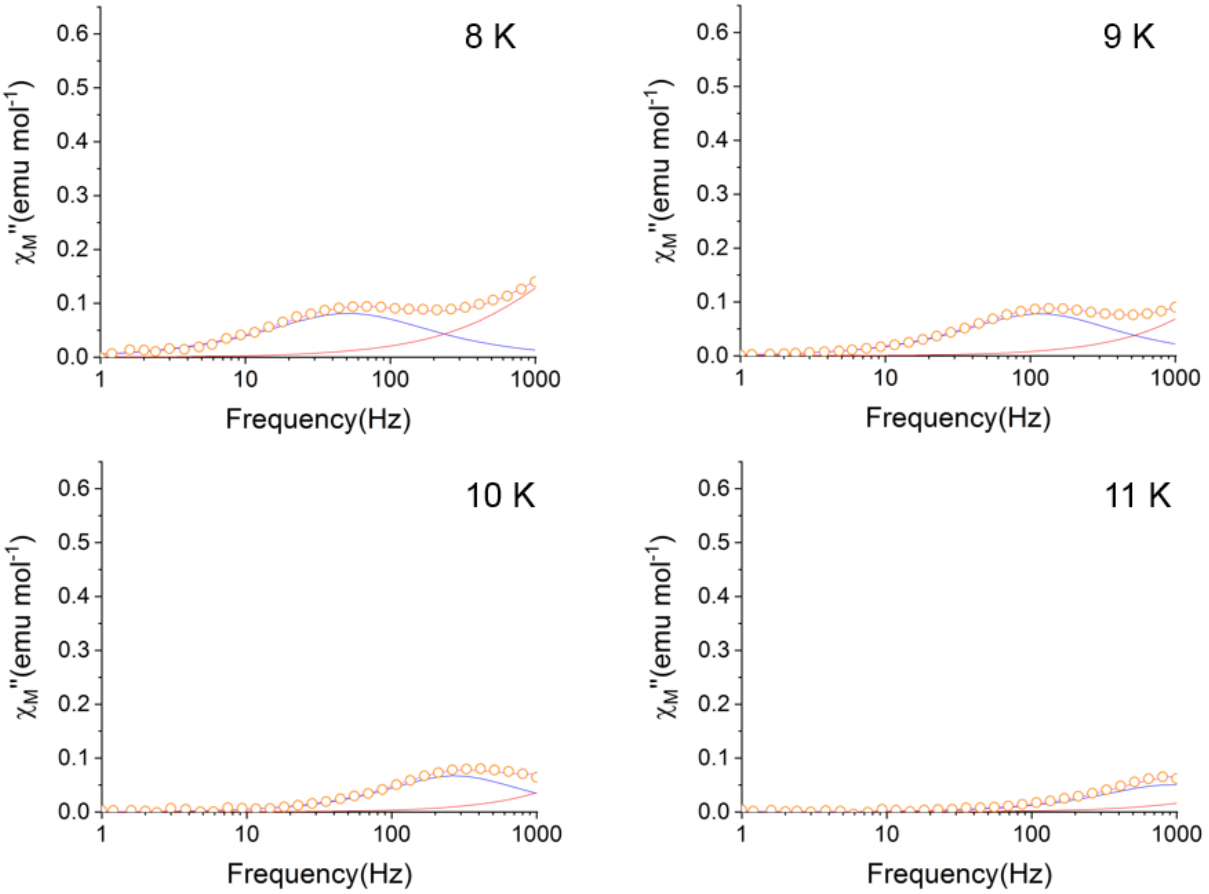

Fig. S36. Frequency dependence of the resolved components of the out-of-phase component of the ac magnetic susceptibility (χ_M'') between 8 K – 11 K for **2-dilute**. Orange circles represent experiment data and lines represent full fit (violet) and resolved fast (red) and slow (blue) relaxation processes.

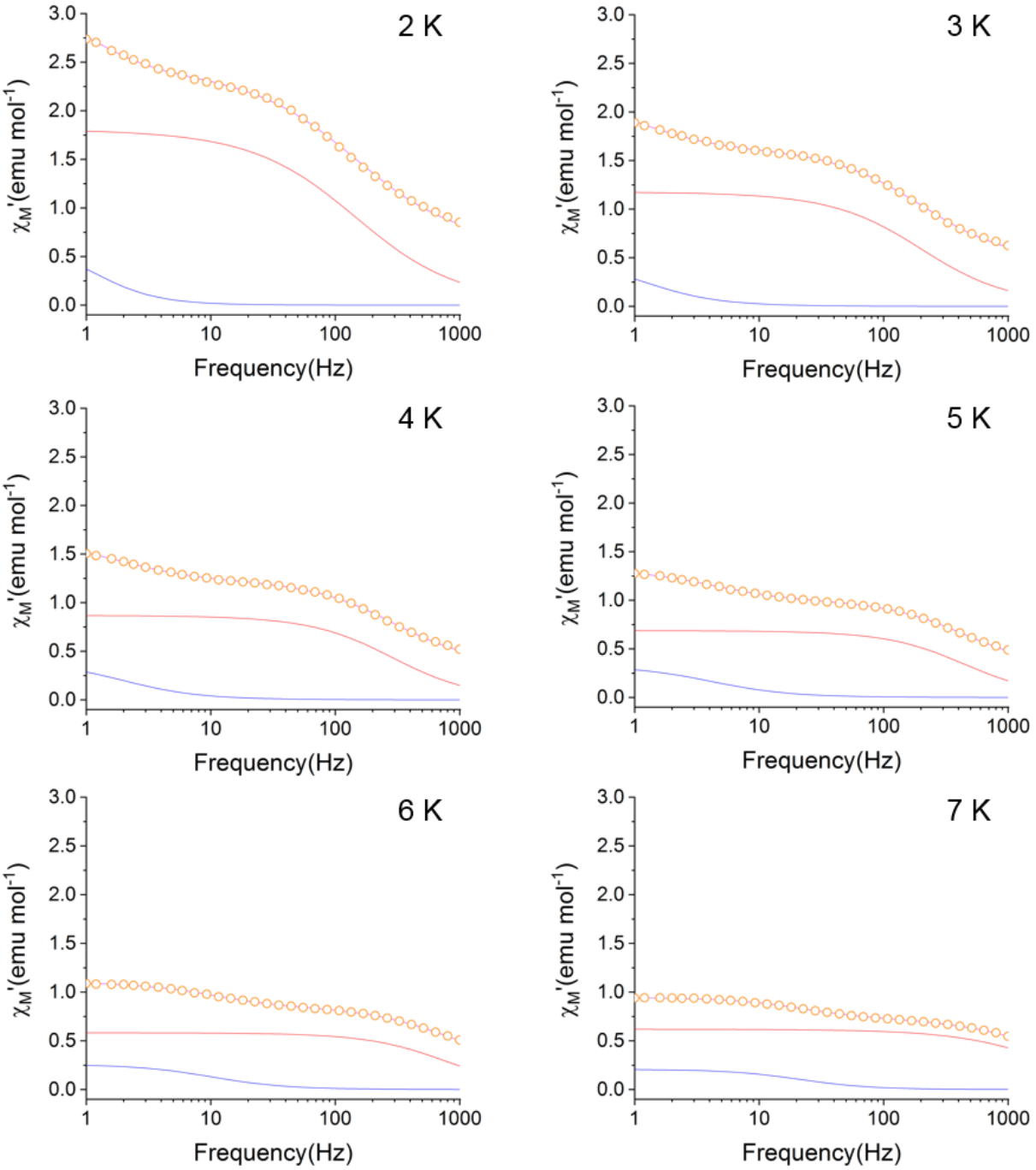

Fig. S37. Frequency dependence of the resolved components of the out-of-phase component of the ac magnetic susceptibility (χ_M') between 2 K – 7 K for **2-dilute**. Orange circles represent experiment data and lines represent full fit (violet) and resolved fast (red) and slow (blue) relaxation processes.

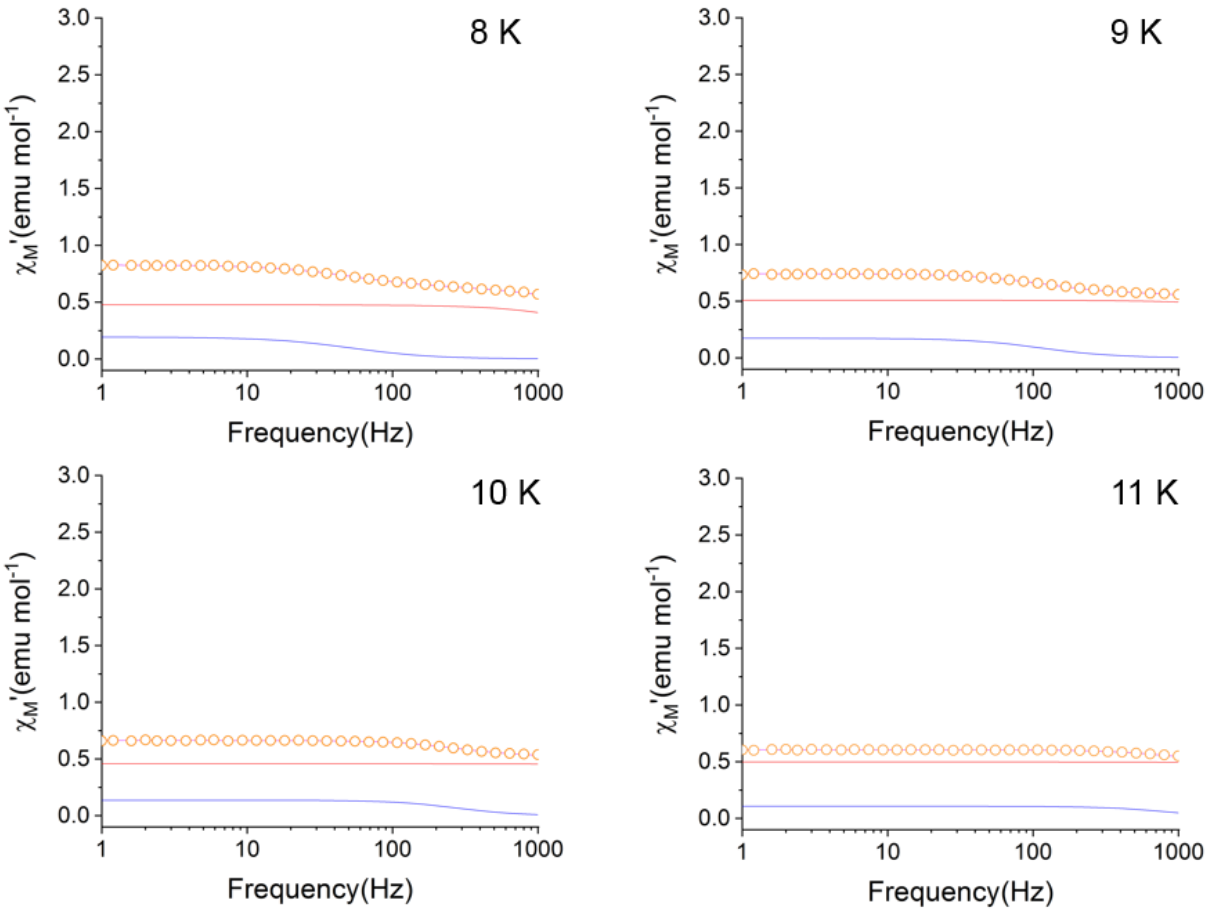

Fig. S38. Frequency dependence of the resolved components of the out-of-phase component of the ac magnetic susceptibility (χ_M') between 8 K – 11 K for **2-dilute**. Orange circles represent experiment data and lines represent full fit (violet) and resolved fast (red) and slow (blue) relaxation processes.

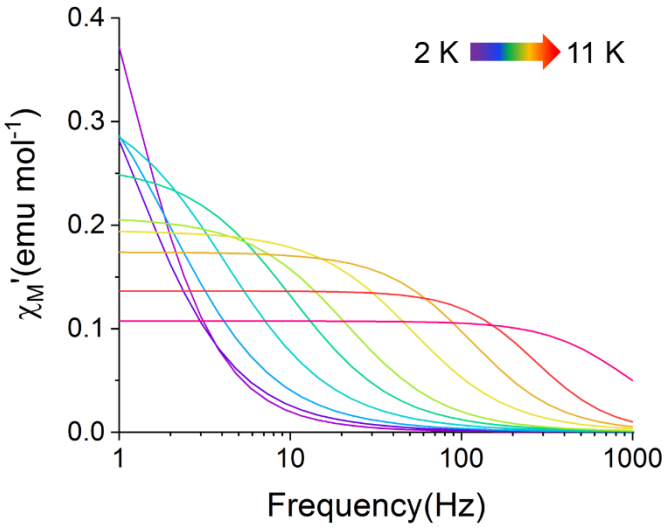

Fig. S39. Temperature dependence of resolved slow relaxation process **(SR)** of the in-phase component of the molar ac magnetic susceptibility (χ_M') of **2-dilute** where H = 0 T and T = 2 - 11 K.

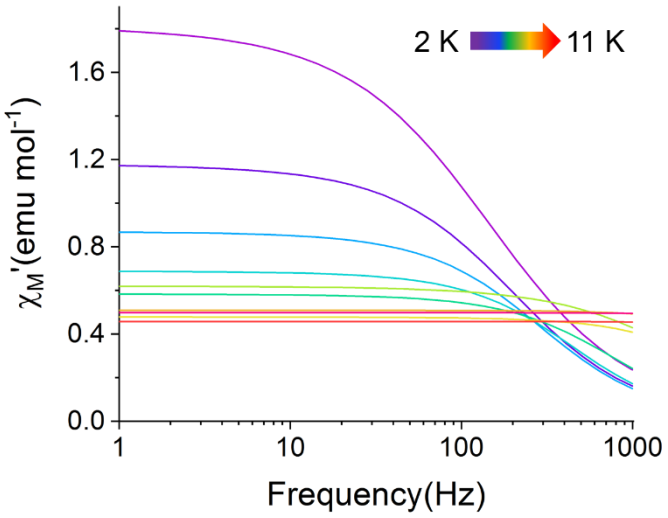

Fig. S40. Temperature dependence of resolved slow relaxation process **(FR)** of the in-phase component of the molar ac magnetic susceptibility (χ_M') of **2-dilute** where H = 0 T and T = 2 - 11 K.

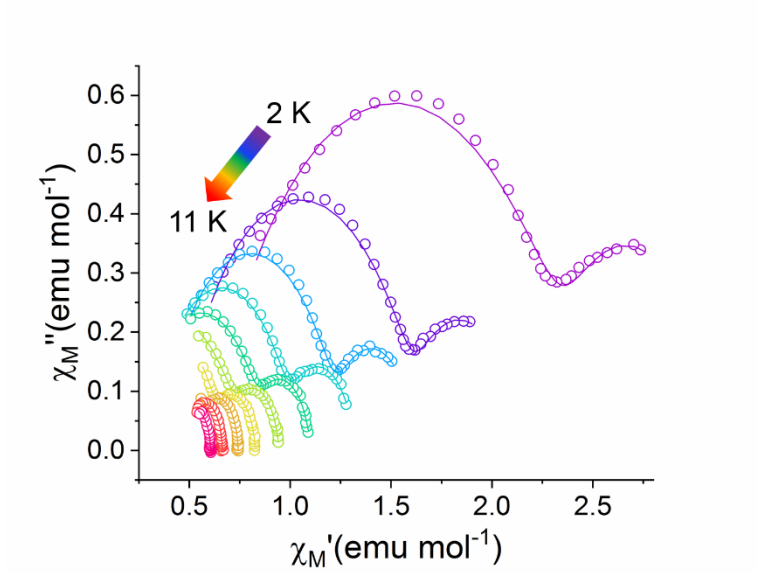

Fig. S41. Cole-Cole plot (χ_M'' vs. χ_M') of **2-dilute** where H = 0 T and T = 2 – 11 K. Lines represent fits to experimental data (circles).

Table S17. Cole-Cole fitting parameters for **[$Ho_{0.06}Y_{0.94}Fc_3(THF)_2Li_2$]$^-$**

T(K)	$\chi_{s,tot}$	$\Delta\chi_1$	τ_1	α_1	$\Delta\chi_2$	τ_2	α_2
2	0.597891	0.652407	0.135	0.0630	1.81183	0.00109	0.275114
3	0.447379	0.48674	0.128	0.125	1.17831	0.000791	0.213673
4	0.357545	0.396793	0.0799	0.145	0.869563	0.000552	0.17854
5	0.305	0.329	0.0383	0.158	0.688	0.000359	0.156
6	0.258653	0.260018	0.0156	0.139	0.583394	0.000206	0.159373
7	0.116556	0.208469	0.00747	0.114	0.619627	0.0000784	0.224438
8	0.154	0.195	0.00307	0.113	0.478	0.0000466	0.123
9	0.0595782	0.174088	0.00138	0.0676	0.508862	0.0000200	0.055366
10	0.0689228	0.136346	0.000585	0.00736	0.457562	0.0000126	6.06E-08
11	1.40E-08	0.107422	0.000172	0.0360	0.49821	0.00000383	0.089157

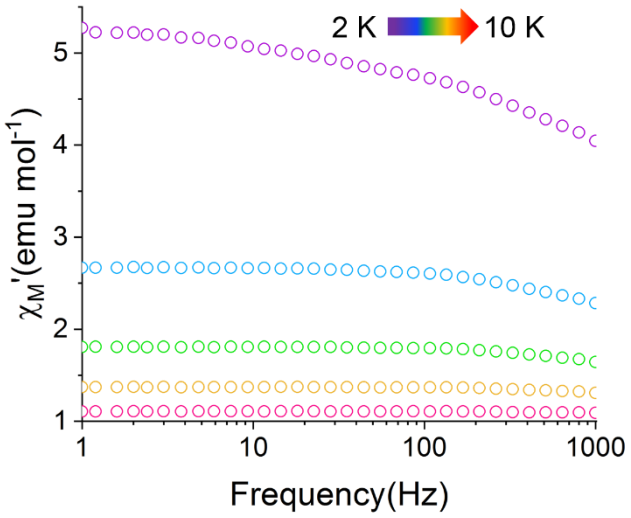

Fig. S42. Temperature dependence of the in-phase component of the molar ac magnetic susceptibility (χ_M') of **2-py** where H = 0 T and T = 2 K – 10 K.

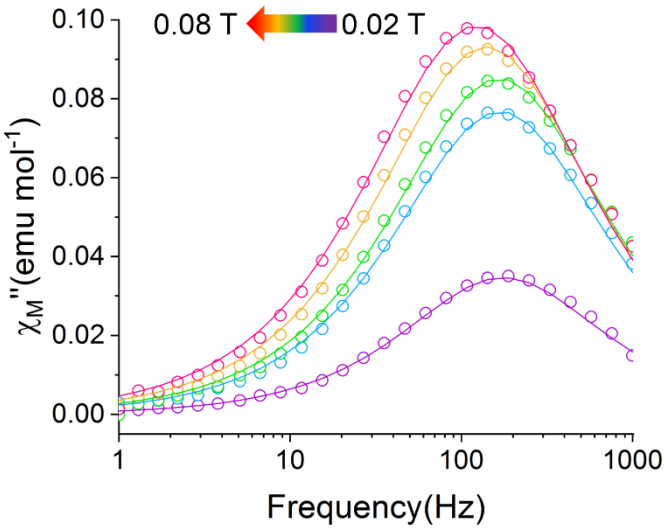

Fig. S43. Field dependence of the out-of-phase component of the molar ac magnetic susceptibility (χ_M'') of **5** where H = 0.02 T – 0.08 T and T = 2 K. Lines represent fit to the experimental data (circles).

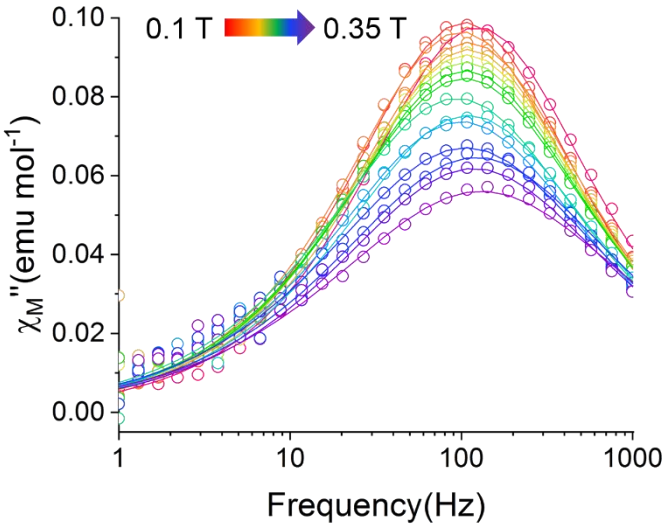

Fig. S44. Field dependence of the out-of-phase component of the molar ac magnetic susceptibility (χ_M'') of **5** where H = 0.1 T – 0.35 T and T = 2 K. Lines represent fit to the experimental data (circles).

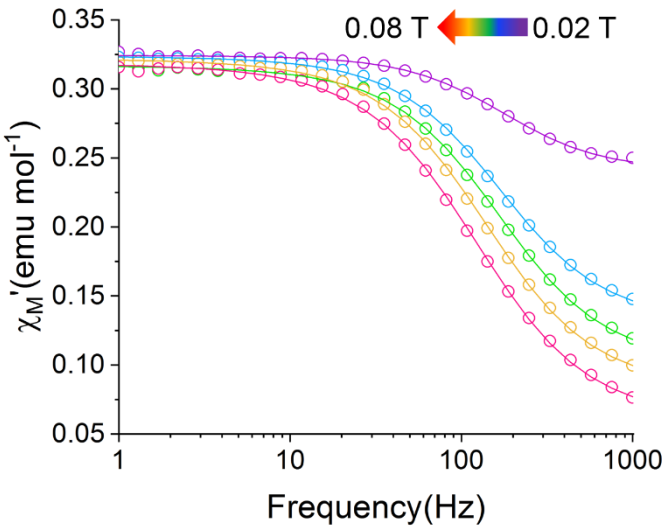

Fig. S45. Field dependence of the in-phase component of the molar ac magnetic susceptibility (χ_M') of **5** where H = 0.02 T – 0.08 T and T = 2 K. Lines represent fit to the experimental data (circles).

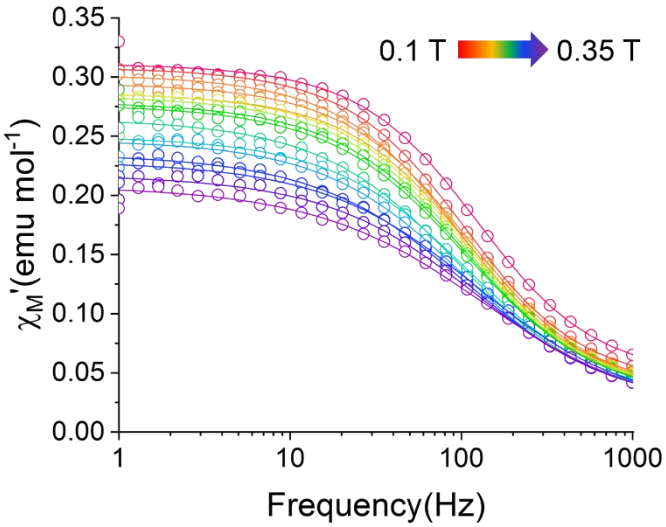

Fig. S46. Field dependence of the in-phase component of the molar ac magnetic susceptibility (χ_M') of **5** where H = 0.1 T – 0.35 T and T = 2 K. Lines represent fit to the experimental data (circles).

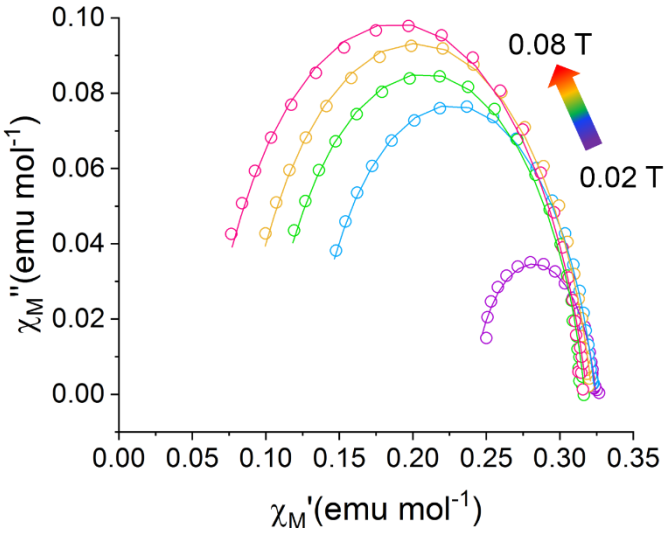

Fig. S47. Cole-Cole plot (χ_M''vs. χ_M') of **5** where H = 0.02 T - 0.08 T and T = 2 K. Lines represent fits to experimental data (solid circles).

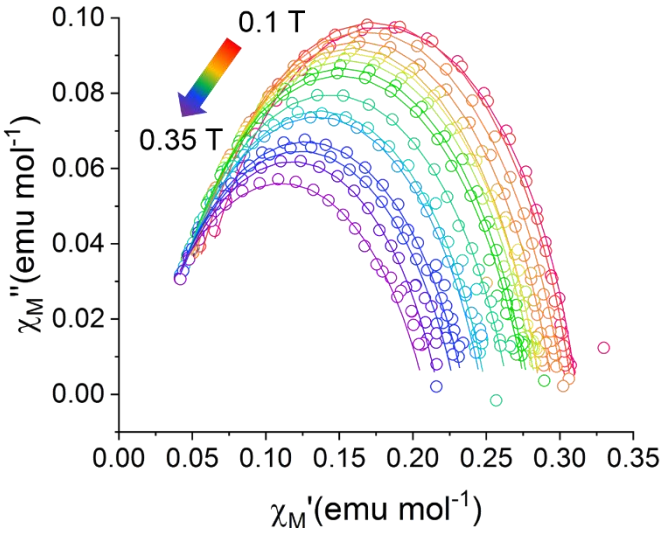

Fig. S48. Cole-Cole plot (χ_M''vs. χ_M') of **5** where H = 0.1 T - 0.35 T and T = 2 K. Lines represent fits to experimental data (solid circles).

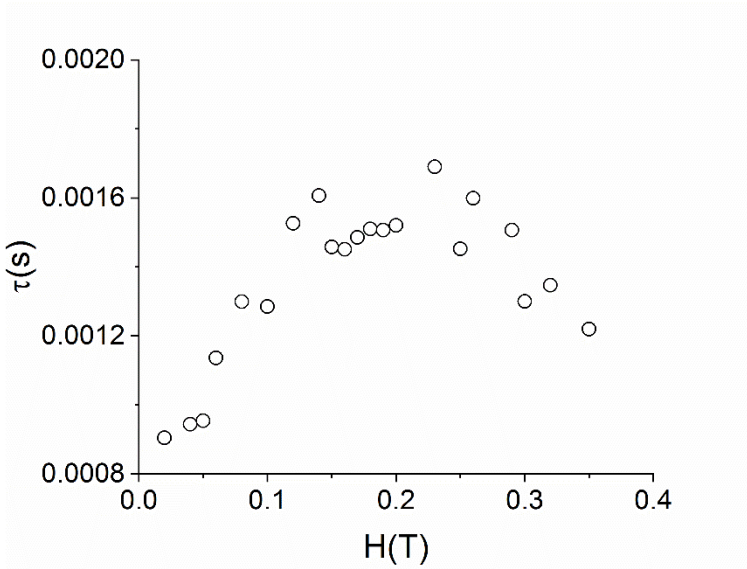

Fig. S49. Plot of the magnetic relaxation time vs. external magnetic field (τ vs. H) of **5** where T = 2 K.

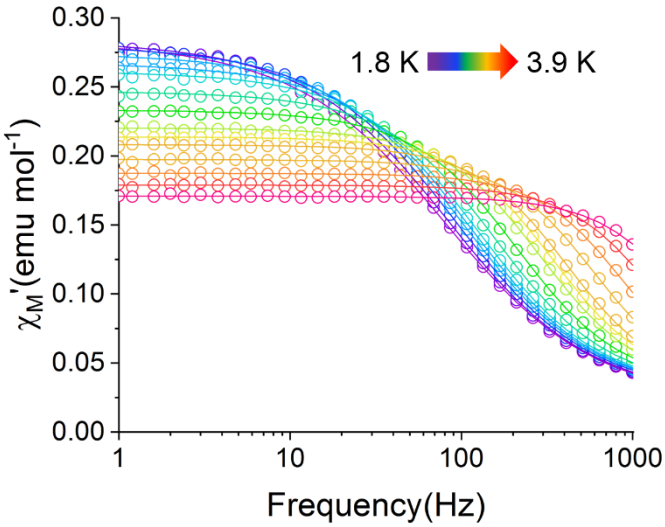

Fig. S50. Temperature dependence of the in-phase component of the molar ac magnetic susceptibility (χ_M') of **5** where H = 0.2 T and T = 1.8 K – 3.9 K. Lines represent fits to experimental data (solid circles).

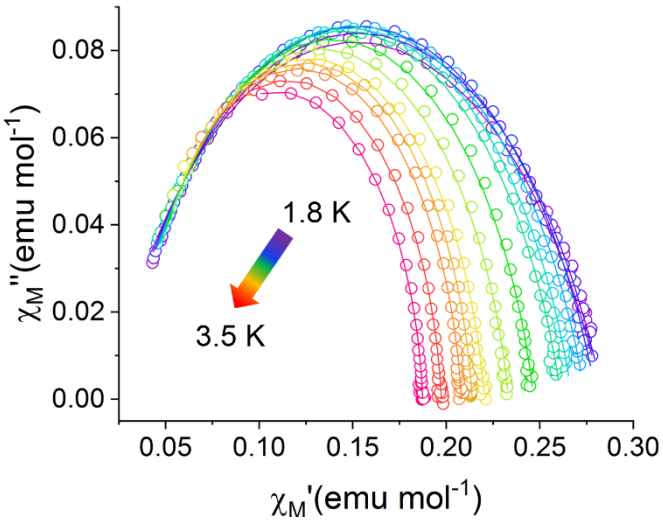

Fig. S51. Cole-Cole plot (χ_M''vs. χ_M') of **5** where H = 0.2 T and T = 1.8 K – 3.9 K. Lines represent fits to experimental data (solid circles).

Table S18. Cole-Cole fitting parameters for **5/5^{Iso}**

T(K)	χ_T	χ_s	τ_1	α_1
1.8	0.283287	0.019272	0.001974	0.292872
1.9	0.283902	0.021639	0.001895	0.2744
2	0.280444	0.024319	0.001713	0.249802
2.1	0.274563	0.025809	0.001542	0.232093
2.2	0.267422	0.027475	0.001396	0.213728
2.3	0.26142	0.028692	0.001264	0.19988
2.5	0.246849	0.03085	0.000994	0.16881
2.7	0.233332	0.032114	0.000751	0.141291
2.9	0.220433	0.032736	0.000545	0.115327
3	0.213904	0.034628	0.000462	0.094887
3.1	0.208131	0.034017	0.000386	0.087193
3.3	0.197373	0.033187	0.000266	0.072814
3.5	0.1874	0.031585	0.000181	0.062496

Table S19. Arrhenius fitting parameters for compounds **5/5^{Iso}** where H = 0.2 T**.**

$[YbFc_3(THF)_2Li_2]^-$ (H = 0.2 T)	
A ($S^{-1}T^{-2}K^{-1}$)	0.304
n_1	4
τ_{QTM} (s)	0.00269
C ($s^{-1}K^{-n}$)	0.00812
n_2	4.25
τ_o (s)	9.04 x 10^{-5}
U (cm^{-1})	6

Multi-configuration Ab Initio Computational Methods

The calculations were carried out using the Molcas 8.2 package program. The Cholesky decomposition threshold was set to $1.0 \cdot 10^{-8}$ to save disk space. The spin-free wave functions and corresponding energies were calculated within multiconfigurational self-consistent field (CASSCF) method. Dynamical electron correlation effects were considered within XMS-CASPT2 calculations. The spin-orbit interaction was taken into account within the restricted active space state interaction (SO-RASSI) method. Magnetic properties were calculated within SINGLE_ANISO program by using the spin-orbital states obtained earlier.

The investigated complexes were calculated in two basis set approximations (Table S20). The active space of the CASSCF method included 10 electrons for Ho complex, 11 electrons for the Er complex, 12 electrons for Tm complex and 13 electrons for the Yb complex, respectively, spanned by seven 4-*f* orbitals. XMS-CASPT2 calculations were performed only on the ground multiplet ^{5}I of Ho(III) (13 roots) and ^{4}I of Er(III) (13 roots), due to high computational cost of CASPT2. Nevertheless, this is justified as these multiplets are well-separated from the excited states.

In case of CASSCF calculations, 35 quintet (all), 106 (out of 210) triplet and 75 (out of 196) singlet states of Ho(III) and 35 quartet (all) and 112 (all) doublet states were mixed by spin-orbit coupling within the module RASSI. In case of CASPT2 calculation, only 13 roots were mixed by spin-orbit coupling. For Tm and Yb complexes all multiplets were mixed by spin-orbit coupling within the module RASSI.

Table S20. Employed Basis Sets For **2-5**

Basis Set 1	**Basis Set 2**
Ln.ANO-RCC-VDZP	Ln.ANO-RCC-VTZP
C.ANO-RCC-VDZP (closest atoms)	C.ANO-RCC-VTZP (closest atoms)
Li.ANO-RCC-VDZP	Li.ANO-RCC-VTZP
Fe.ANO-RCC-VDZ	Fe.ANO-RCC-VDZP
O.ANO-RCC-VDZ	O.ANO-RCC-VDZP
C.ANO-RCC-VDZ (the rest)	C.ANO-RCC-VDZP (the rest)
H.ANO-RCC-VDZ	H.ANO-RCC-VDZP

Table S21. Energy of low-lying Ising doublets of **2**.

Ho(1)			Ho(2)		
CASSCF/SO-RASSI		**XMS-CASPT2/SO-RASSI**	**CASSCF/SO-RASSI**		**XMS-CASPT2/SO-RASSI**
Basis Set 1	**Basis Set 2**	**Basis Set 1**	**Basis Set 1**	**Basis Set 2**	**Basis Set 1**
0	0	0	0	0	0
0.0163	0.0146	0.1325	0.0058	0.0040	0.0591
87.7640	89.9123	137.0824	87.2834	89.1908	130.6269
88.0859	90.2286	137.1925	87.6955	89.5925	131.3987
123.7440	126.6218	227.7217	108.1905	110.8759	203.2110
123.7725	126.6497	228.2524	108.2036	110.8884	203.4200
248.4775	254.4482	389.3542	252.4162	258.7200	397.3983
248.8462	254.8210	390.5907	252.6976	258.9938	397.8657
302.7721	309.1171	424.9725	294.3894	300.1872	407.3960
307.2236	312.9093	433.2938	295.9709	301.7161	421.0204
311.0652	317.1463	447.0406	296.8573	302.4243	425.4788
344.4284	351.1120	504.8665	339.0885	345.1940	492.3853
351.5471	357.9034	516.2164	341.9988	348.2468	498.7415
354.5961	360.9895	522.8741	349.0398	355.6887	515.0601
360.6889	367.2209	537.9741	351.4742	358.1419	524.3168
365.3192	371.7621	540.7899	353.0931	359.3979	527.0679
371.8681	378.7497	565.8972	367.0136	374.1872	553.4065
…	…	…	…	…	…

Table S22. The g-tensor of the lowest four doublets of **2**.

Doublet		**Ho(1)**			**Ho(2)**		
		CASSCF/SO-RASSI		**XMS-CASPT2/SO-RASSI**	**CASSCF/SO-RASSI**		**XMS-CASPT2/SO-RASSI**
		Basis Set 1	**Basis Set 2**	**Basis Set 1**	**Basis Set 1**	**Basis Set 2**	**Basis Set 1**
1	g_x	0	0	0	0	0	0
	g_y	0	0	0	0	0	0
	g_z	17.256	17.255	17.400	17.154	17.150	17.313
2	g_x	0	0	0	0	0	0
	g_y	0	0	0	0	0	0
	g_z	15.183	15.140	15.025	14.826	14.807	14.864
3	g_x	0	0	0	0	0	0
	g_y	0	0	0	0	0	0
	g_z	18.161	18.146	17.774	17.837	17.804	17.364
4	g_x	0	0	0	0	0	0
	g_y	0	0	0	0	0	0
	g_z	13.837	13.877	14.354	14.292	14.334	14.737

Table S23. Energy of low-lying Kramers doublets of **3**.

Er(1)			Er(2)		
CASSCF/SO-RASSI		XMS-CASPT2/SO-RASSI	CASSCF/SO-RASSI		XMS-CASPT2/SO-RASSI
Basis Set 1	**Basis Set 2**	**Basis Set 1**	**Basis Set 1**	**Basis Set 2**	**Basis Set 1**
0	0	0	0	0	0
15.5838	15.5437	28.3174	22.8589	23.1214	44.5408
24.2677	24.6167	52.3575	29.4734	30.7615	59.3961
67.9016	68.9957	133.0082	78.6221	80.2467	130.1299
125.6077	129.2564	151.2557	115.9929	119.5765	153.2307
291.7105	300.5894	372.2061	305.2271	312.4205	406.8919
309.4177	316.8159	433.3370	312.2808	321.6642	442.3643
418.3933	427.6462	603.7203	418.4531	427.7902	608.1374
…	…	…	…	…	…

Table S24. The g-tensor of the lowest four doublets of **3**.

Doublet		Er(1)			Er(2)		
		CASSCF/SO-RASSI		XMS-CASPT2/SO-RASSI	CASSCF/SO-RASSI		XMS-CASPT2/SO-RASSI
		Basis Set 1	**Basis Set 2**	**Basis Set 1**	**Basis Set 1**	**Basis Set 2**	**Basis Set 1**
1	g_x	1.325	1.398	9.997	8.919	8.812	9.259
	g_y	3.578	3.711	7.516	8.206	8.366	8.935
	g_z	11.598	11.386	0.150	0.618	0.574	1.346
2	g_x	0.177	0.198	2.156	4.415	4.063	9.493
	g_y	3.612	3.209	4.736	3.189	3.284	7.142
	g_z	10.464	10.287	8.965	1.482	1.539	0.039
3	g_x	0.979	0.902	4.983	0.163	0.024	0.694
	g_y	3.797	3.332	3.382	3.934	4.191	1.205
	g_z	8.451	8.631	0.736	9.280	8.974	5.426
4	g_x	4.525	4.701	10.797	7.787	7.663	1.505
	g_y	6.410	6.368	6.514	7.643	7.581	1.737
	g_z	8.337	8.090	1.797	4.233	4.345	11.780

Table S25. Energy of low-lying Ising doublets of **4**.

Tm(1)			Tm(2)	
CASSCF/SO-RASSI		**XMS-CASPT2/SO-RASSI**	**CASSCF/SO-RASSI**	
Basis set 1	**Basis set 2**	**Basis Set 1**	**Basis set 1**	**Basis set 2**
0	0	0	0	0
53.7197	54.1470	86.9322	64.8622	63.9215
77.4835	75.8293	115.6344	67.1481	67.4462
229.0314	227.2171	348.8809	231.8079	230.6903
235.1374	233.4589	359.4642	234.9476	233.9113
425.2806	423.2648	614.8964	418.4029	416.9864
427.1032	424.7643	628.4261	430.6369	429.1841
587.8185	587.0609	793.9510	581.4877	581.3949
588.0892	587.3857	794.4556	581.6486	581.6125
729.4138	731.0481	912.2663	714.4138	716.3315
729.4599	731.0980	912.3256	714.4469	716.3688
976.3267	975.4922	1196.5839	939.2977	938.2321
976.3328	975.4987	1196.5971	939.3018	938.2370
7033.6717	7084.8159	6103.0014	7008.3906	7058.7104
7034.5591	7085.7176	6106.8661	7009.0430	7059.4685
…	…	…	…	…

Table S26. Energy of low-lying Kramers doublets of **5**.

Yb(1)			Yb(2)	
CASSCF/SO-RASSI		**XMS-CASPT2/SO-RASSI**	**CASSCF/SO-RASSI**	
Basis set 1	**Basis set 2**	**Basis set 1**	**Basis set 1**	**Basis set 2**
0	0	0	0	0
87.9764	122.7001	122.7001	17.0556	18.8225
350.4011	475.9593	475.9593	308.9726	308.0120
911.6152	1208.0192	1208.0192	862.8261	864.1961
10437.7246	10479.2524	10479.2524	10415.9948	10287.2058
10589.8561	10636.9361	10636.9361	10539.8952	10413.0392
11219.6615	11490.9949	11490.9949	11172.3365	11046.4576

Table S27. The g-tensor of the lowest four doublets of **5**.

Doublet		**Yb(1)**			**Yb(2)**	
		CASSCF/SO-RASSI		**XMS-CASPT2/SO-RASSI**	**CASSCF/SO-RASSI**	
		Basis Set 1	**Basis Set 2**	**Basis Set 1**	**Basis Set 1**	**Basis Set 2**
1	g_x	1.229	0.949	1.847	0.369	0.790
	g_y	1.948	1.646	2.645	1.229	2.530
	g_z	6.883	7.135	4.920	6.271	5.781
2	g_x	1.074	1.352	0.425	4.724	0.499
	g_y	2.577	2.830	0.677	3.375	2.016
	g_z	6.283	6.002	6.893	0.884	4.038
3	g_x	0.001	0.001	0.042	0.044	0.051
	g_y	0.184	0.152	0.336	0.300	0.278
	g_z	5.491	5.491	5.298	5.375	5.364
4	g_x	0.031	0.046	0.084	0.033	0.048
	g_y	0.032	0.048	0.087	0.033	0.048
	g_z	7.992	7.992	7.987	7.991	7.991

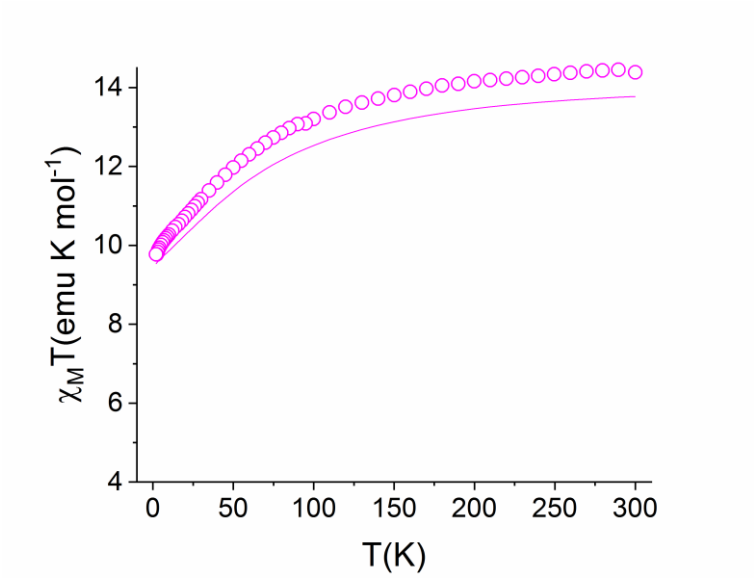

Fig. S52. Experimental (circles) vs. CASPT2 calculated (solid line) temperature dependence of the molar magnetic susceptibility temperature product ($\chi_M T$) of **Ho(1)** of **2** where H = 0.1 T and T = 300 K – 2K

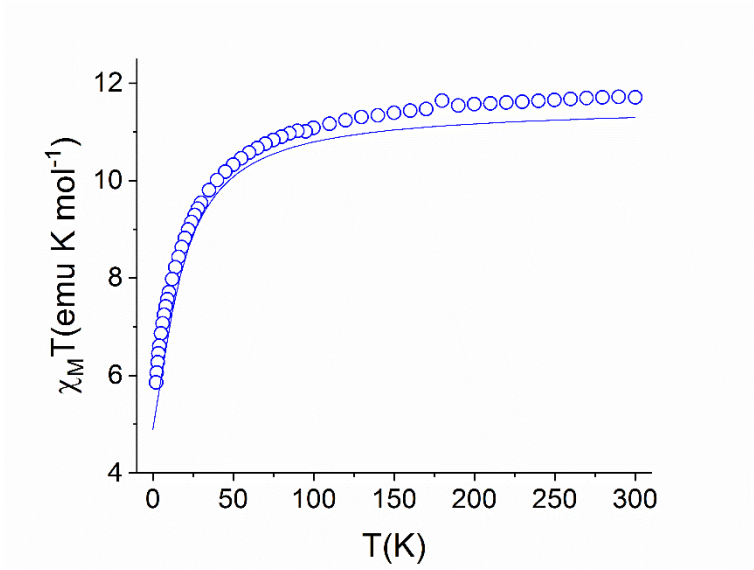

Fig. S53. Experimental (circles) vs. CASPT2 calculated (solid line) temperature dependence of the molar magnetic susceptibility temperature product ($\chi_M T$) of **Er(2)** of **3** where H = 0.1 T and T = 300 K – 2K.

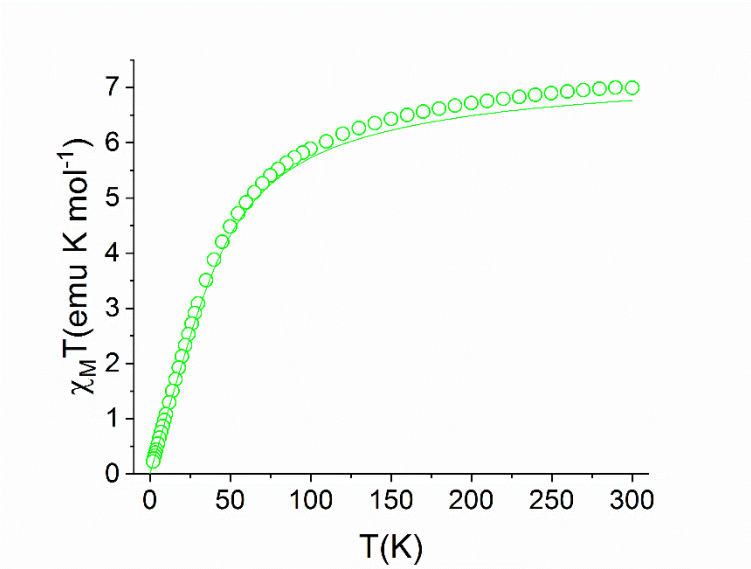

Fig. S54. Experimental (circles) vs. CASPT2 calculated (solid line) temperature dependence of the molar magnetic susceptibility temperature product (χ_MT) of **Tm(1)** of **4** where H = 0.1 T and T = 300 K – 2K.

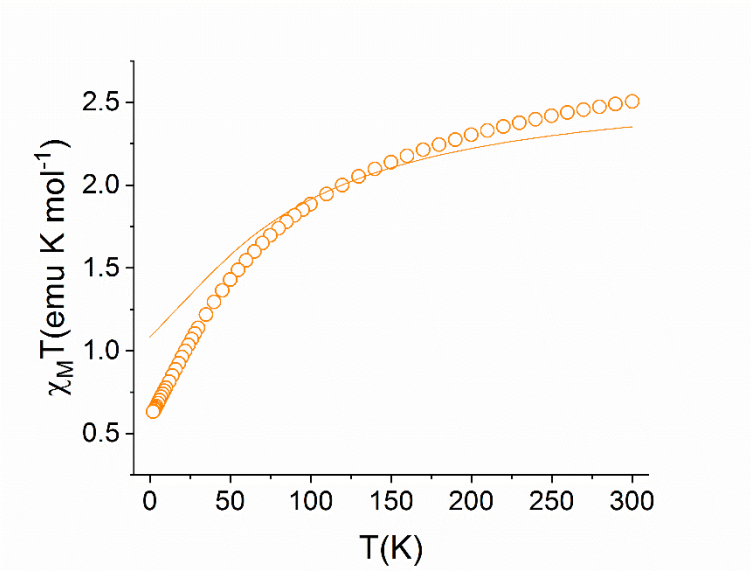

Fig. S55. Experimental (circles) vs. CASPT2 calculated (solid line) temperature dependence of the molar magnetic susceptibility temperature product (χ_MT) of **Yb(1)** of **5** where H = 0.1 T and T = 300 K – 2K.

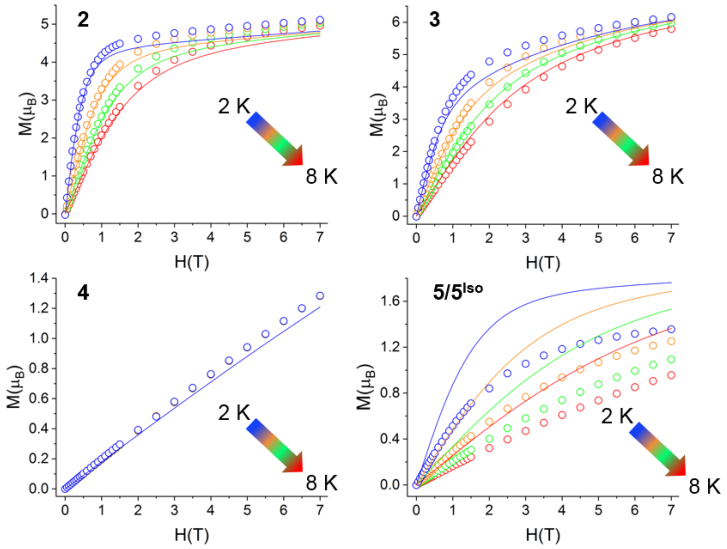

Fig. S56. Experimental (circles) vs. CASPT2 calculated (solid lines) M vs. H curves for the **2, 4** and **5 of Ln(1)** and **3** of **Er (2)** where H = 0 – 7 T and T = 8 K – 2K.

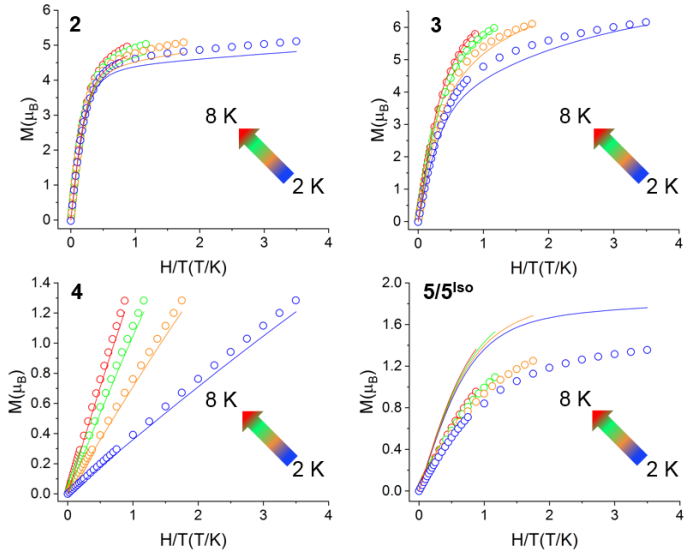

Fig. S57. Experimental (circles) vs. CASPT2 calculated (solid lines) M vs. H/T curves for the **2, 4** and **5 of Ln(1)** and **3** of **Er (2)** where H = 0 – 7 T and T = 8 K – 2K.

References

(1) APEX3 “Program for Data Collection on Area Detectors” BRUKER AXS Inc., 5465 East Cheryl Parkway, Madison, WI 53711-5373 USA.

(2) SADABS, Sheldrick, G.M. “Program for Absorption Correction of Area Detector Frames”, BRUKER AXS Inc., 5465 East Cheryl Parkway, Madison, WI 53711-5373 USA.

(3) a).G.M. Sheldrick, *Acta Cryst.* 2008, **A64**, 112-122. b) G.M. Sheldrick, *Acta Cryst.* 2015, **A71**, 3-8. G.M. Sheldrick, Acta Cryst. 2015, **C71**, 3-8. XT, XS, BRUKER AXS Inc., 5465 East Cheryl Parkway, Madison, WI 53711-5373 USA.

(4) A.L. Spek, "PLATON - A Multipurpose Crystallographic Tool" *J. Appl. Cryst.* 2003, **36**, 7-13.; Spek, A. L., Utrecht University, Utrecht, The Netherlands 2008.

(5) O.V. Dolomanov, L.J. Bourhis, R.J. Gildea, J.A.K. Howard,H. Puschmann, “OLEX2: A Complete Structure Solution, Refinement and Analysis Program”, *J. Appl. Cryst.* 2009, **42**, 339-341.